Investigation of the Mechanism of Protein Denaturation by Urea Through a Judicious Selection of Model Systems

By

Simisola Ajayi

A Thesis submitted to the Faculty of Graduate Studies of

The University of Manitoba

in partial fulfilment of the requirements of the degree of

MASTER OF SCIENCE

Department of Chemistry

University of Manitoba

Winnipeg

Table of Contents

Abstract

Currently, urea is widely believed to unfold proteins by increasing the solubility of the amide backbone through direct interactions rather than through global changes in solvent water structure. Urea is thought to enhance hydrogen bonding or van der Waals interactions, thereby increasing the solubility of the amide backbone. However, there are few experimental data to confirm any of these proposed mechanisms. In this work, we first investigated the effects of urea addition on the hydrogen bonding network of water by measuring how it perturbs the fluorescence spectra of the 1-aminonaphthalene (1-AN) and 1-dimethylaminonaphthalene (1-DMAN) molecules involved in hydrogen bonding. In both cases, the fluorescence spectra of the two molecules show that the hydrogen bonding properties of the solvent are minimally affected by the addition of urea from the solute point of view. We have also studied the effects of urea addition on intra-molecular hydrogen bonding as represented by the carboxylate-hydroxyl bond in salicylic acid. Our measurements show that the addition of urea has no effect on the strength of the intra-molecular hydrogen bonds. Finally, we investigate how the addition of urea perturbs the solvation energy of amide moieties in water by comparing the urea-induced changes in the solubility of acetaminophen and 4-tertbutylphenol. Our measurements show that the addition of urea has no appreciable effect on the hydrogen bonding interactions between amide and solvent. Rather, we show that the increase in amide solvation enthalpy correlates linearly with the change in solvent packing density. This confirms the enhanced van der Waals interactions between the solvent and dissolved amide groups in binary urea-water mixtures (relative to pure water). The results of work presented here clearly confirm the theoretical calculations that identify an increase in van der Waals interactions between solvent and amide as the main mechanism for protein denaturation.

Keywords: urea, H-bonding, van der Waals, amide, solubility.

Acknowledgements

I would like to thank my supervisor and P.I. Dr. Mazdak Khajehpour for his guidance and support throughout the course of my graduate studies in his research laboratory at the University of Manitoba. Thank you for being there every day with us, and being as hands-on and involved as you are. It definitely motivated me to work hard and played a huge part in my success. To Iman, Hanieh and Bahareh; thank you all for your help in the lab and for all the fun times, I will never forget you guys, my Iranian family. Thank you Dr. Dave Davidson for all your help with the setting up the Flourine NMR experiments and data analysis. Finally, I thank my esteemed committee members Dr. Sean McKenna and Dr. Ned Budisa for their time, thoughtful insights and valued contributions to my thesis. This work was supported by Natural Sciences and Engineering Research Council of Canada (NSERC) grant 2017-05935 (to M. K.) and a Canadian Foundation for Innovation (CFI) grant (23175).

Dedication

My journey as a Master's student has been very interesting to say the least. Though I did learn a lot about doing research, I found that the most impactful lessons that came out of this experience had nothing to do with the technical things. A lot of hard work went into the fruition of this thesis, which in turn built a lot of character and fortitude. I am so thankful for the woman I have become, and very glad that it all worked out the way it did. I dedicate this thesis to my doting family, dear friends, and all those who wish me well. It was truly a pleasure. Love, Simi.

List of Abbreviations

1. **1-AN:** 1-aminonaphthalene
2. **1-DMAN:** 1-dimethylaminonaphthalene
3. **ACN:** acetonitrile
4. **H-bonding:** hydrogen bonding
5. **NMR:** Nuclear Magnetic Spectroscopy
6. **ORF:** Onsager Reaction Field
7. ***o*-HBA**: *o*-hydroxybenzoic acid
8. ***p*-4HBA:** *p*-hydroxybenzoic acid
9. **vdW:** van der Waals

List of Tables

Table 8. Parameters required or calculated for scaled particle theory analysis of the solubility data (abbreviations: ACT (acetaminophen); TBP (4-tertbutylphenol) [61, 112, 119-127].

List of Figures

Chapter 1: Introduction to Protein Denaturation

Chapter 2: Materials & Methods

Chapter 3: Results & Discussion

Part I: Determination of the Effects of Urea Addition on H-bonding Donor/Acceptor Properties of Aqueous Solvent Systems

density of hard particle centers in contact with the cavity surface is denoted by ρG(λ, ρ). Adapted from Corti (2004) [128].

Figure 21. Effects of urea (blue) and acetonitrile (red) addition upon the cavitation free-energies of acetaminophen (squares) and 4-tertbutylphenol (circles), as a function of the change in packing density of the solvent system ξ.

Figure 22. ΔΨ plotted as a function of the change in packing density of the solvent system for urea (blue) and acetonitrile (red).

Chapter 1.

Introduction to Protein Denaturation

1.1. What is Protein Denaturation?

Proteins are dynamic biomolecules that can adopt a range of conformations, and their biological activity depends on their native 3-dimensional structure which allows them to carry out their function [1-3]. The native state structure is based on the amino acid sequence encoded in its polypeptide chain. However, the folding process also depends on the protein's microenvironment and other physicochemical conditions [1-4].

Denaturation is the physical process by which the native structure of a protein or peptide is disrupted *in vivo* or *in vitro*, and biological function is lost due to external stresses such as extreme pH, temperature, ionic strength and chemical denaturants [5-8]. The integrity of the polypeptide chain is still maintained; therefore, the protein is said to be destabilized or unfolded, and not degraded [5-8].

Under non-physiological conditions, proteins may unfold, aggregate, or undergo alternative folding transitions which may result in non-native structures (i.e., misfolding) [2,9]. Such occurrences may lead to a myriad of dysfunctions and diseases in organisms, e.g. prions and amyloid proteins [2,9]. The interactions involved in the denaturation of proteins are likely very different from those involved in protein folding processes, or even between the denaturants themselves. This is even seen in the differential chemical denaturation of proteins by urea and guanidium hydrochloride [21]. Moreover, biophysical studies relating to protein stability in various microenvironments make use of thermodynamic functions and parameters which may only really

be determined by intentionally perturbing the native state. Therefore, understanding the process of chemical denaturation is of central importance to bioscience [2,3,5].

1.2. Protein Folding Energetics

In solution, a dynamic equilibrium exists between the native (F) and unfolded (U) conformations of a protein which can be characterized by thermodynamic parameters [2,4,5-8]. Gibbs free energy (G) is defined as the amount of energy present in a system that is available to be used in a chemical transformation or reaction [2]. If the change in Gibbs free energy (ΔG) for a reaction is negative, it is spontaneous; and vice versa for a positive ΔG value [2]. The stability of a protein is therefore defined as the ΔG of the folding process, as this parameter defines whether the native or the unfolded conformation will be adopted spontaneously [1-5]. Protein stability may also vary drastically depending on its pathway of folding, which may be a one or multi-step process (e.g., with intermediates, molten globules) [1-4]. For the thermodynamics of a one-step folding transition with no intermediates (characteristic of small, monomeric proteins) the folding equilibrium can be expressed as [2,4]:

$$U \underset{k_u}{\overset{k_f}{\rightleftharpoons}} F \qquad (1)$$

Where K_f and K_u are the rate constants of folding and unfolding respectively. The Gibbs standard free energy of folding ($\Delta G^0_{U\rightarrow F}$) can be described with the following equation, where R is the gas constant, T is the temperature, and K_{eq} is the equilibrium constant:

$$\Delta G^0_{U\rightarrow F} = -RT\ln(K_{eq}) = -RT\ln(\frac{k_f}{k_u}) \qquad (2)$$

The concentrations of the native [F] and unfolded [U] protein can be written as:

$$\frac{[F]}{[U]} = \frac{k_f}{k_u} \quad (3)$$

The equilibrium concentrations of the F and U species are reached when they match the rate of conversion from one state to another. Therefore, the unfolding reaction can also be considered as the forward reaction:

$$F \underset{k_f}{\overset{k_u}{\rightleftharpoons}} U \quad (4)$$

The Gibbs standard free energy of unfolding ($\Delta G^0_{F\rightarrow U}$) is given by:

$$\Delta G^0{}_{F\rightarrow U} = -RT\ln\frac{k_u}{k_f} = -\Delta G^0{}_{U\rightarrow F} \quad (5)$$

In thermodynamics, enthalpy (H) is the sum of the system's internal heat energy, and entropy (S) is the degree of disorder or uncertainty in the system [2]. ΔG is related to the change in enthalpy (ΔH) and entropy (ΔS) of a system in equilibrium as described in the following equation [2]:

$$\Delta G^0 = \Delta H^0 - T\Delta S^0 \quad (6)$$

1.3. The Role of Solvation in Protein Denaturation

Protein structure is governed by a delicate interplay between protein-protein interactions, protein-solvent interactions, and solvent-solvent interactions [1-3]. The unfolded state has a larger surface area exposed to the solvent and therefore maintains more protein-solvent contacts, while the native state has an increased number of protein-protein and solvent-solvent contacts [5-8,10]. Some solvent-related factors that regulate protein structure include polarity, hydrogen bonding (H-bonding) abilities, ionic strength, presence of co-solvents [5-8,10].

The major destabilizing force in proteins is the unfavorable conformational entropy of the native state [11,12]. As a protein folds, the conformational flexibility is largely reduced, i.e., the rotation around the many bonds in a protein is much less restricted in the unfolded conformation than in the native conformation [11,12]. This provides a strong entropic force for the unfolding of proteins. However, under physiological conditions, protein-protein and solvent-solvent interactions are generally more favorable than protein-solvent interactions because they decrease the net energy of the system through different enthalpic and entropic mechanisms, driving folding [2,3,5,10].

Enthalpic interactions are direct and pair-specific in nature. Important enthalpic interactions involved in protein folding include H-bonding, dispersion interactions, and various forms of long-range interactions (e.g. disulfide bonding, charge-charge) which stabilize tertiary structure [1-3]. The hydrophobic effect and the excluded volume effect are entropically-driven and act collectively over the system [13,14]. The stability of a native protein is therefore defined as the difference between favorable enthalpic interactions that contribute to its structure, favorable entropic terms, and the unfavorable conformational entropy of the protein [3,5]. Overall, the stabilizing and destabilizing forces in protein folding are both large and almost equal. This means that the native conformation is only slightly more stable (5-15 kcal/mol) than the unfolded conformation [3,5].

1.4. Co-solvents and the F ⇌U Equilibrium

The conformational equilibrium of a protein in solution may be perturbed by changing the thermodynamic state of the system (e.g. temperature, pH, pressure) or by altering the solvent properties/composition. Co-solvents are solvent additives (e.g., organic solvents, osmolytes) that

modulate protein stability by shifting the folding equilibrium to favor the native or unfolded state [5-7]. Osmolytes are small organic molecules that affect protein folding in aqueous environments, *in vivo* and *in vitro* [15-18]. Protecting osmolytes push the folding equilibrium to favor the native state (e.g., trimethylamine-N-oxide, polyols), while denaturing osmolytes favor the unfolded state (e.g., urea, guanidinium hydrochloride) [5-7,15-18]. Additionally, some organic solvents (e.g. alcohols) have been shown to induce the folding of disordered peptides into α-helical structures in aqueous solutions [19]. The interactions between co-solvents and proteins are very weak, i.e., they need to be present in high concentrations to fully invert the populations of the native versus unfolded state [5-8,15].

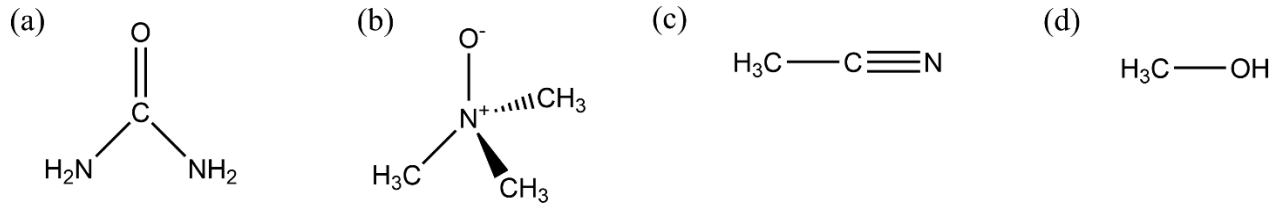

Figure 1. Common co-solvents used in protein folding research. (a) urea, (b) TMAO (c) acetonitrile, (d) methanol.

1.5. Use of Urea as a Denaturant in Protein Folding Research

Urea is a common chemical denaturant which has been extensively used in protein folding research as a stability perturbing agent [5-8, 20-24]. Urea denaturation experiments have helped in understanding the relationship between the structure/dynamics of a protein and its interaction with the microenvironment [20,21,48-51]. Thermodynamic solvation studies of model compounds in water demonstrate that adding urea to water increases the solubility of hydrophobic and amide moieties, causing proteins to unfold [50-52]. However, there is still no consensus view on the exact mechanism of denaturation. First, let us look at the thermodynamics of protein-urea systems and the molecular

interactions thought to be involved. Here I review experimental findings which may be useful in clarifying urea's mechanism of action, with a few insights from theoretical models.

1.5.1. Equilibrium Unfolding of Proteins in Urea Solutions: Urea Decreases $\Delta G_{F\rightarrow U}$

Numerous equilibrium-unfolding studies have been performed on a variety of protein structures, which has provided some insight on how exactly urea destabilizes different types of proteins. Studies show the Gibbs free energy of unfolding ($\Delta G_{F\rightarrow U}$) decreases linearly from a positive to a negative value when urea is added to protein solutions at high concentration, i.e. the unfolding reaction becomes spontaneous [5-8,20-24]. The concentration of urea needed to unfold a specific protein in solution is dependent on the stability of the protein in water, $\Delta G_{F\rightarrow U}^{H20}$, and the relationship between $\Delta G_{F\rightarrow U}$ and urea concentration [5,8,20-27].

For the experimental determination of $\Delta G_{F\rightarrow U}$, the concentration of urea in a protein solution is increased incrementally, such that the protein reaches an equilibrium between the native and unfolded conformation at each concentration used [20]. The equilibrium concentrations of the native ($[F]_{eq}$) and unfolded ($[U]_{eq}$) conformations can be determined at each urea concentration using physical techniques like fluorescence spectroscopy and circular dichroism. For a one-step transition of a monomeric protein, $[F]_{eq} + [U]_{eq} = 1$ [20].

The $\Delta G_{F\rightarrow U}$ cannot easily be determined at low and high concentrations, since the $[U]_{eq}$ and $[F]_{eq}$ ratios create large uncertainties in the equilibrium constants, K_f and K_u [20,22]. The Linear Extrapolation Model (LEM) assumes that the $\Delta G_{F\rightarrow U}$ is a linear function of the denaturant concentration, [D] [22]. Therefore, the $\Delta G_{F\rightarrow U}$ can be extrapolated to zero denaturant concentration using a linear regression of experimental data. This allows for the determination of the free energy of unfolding in water, $\Delta G_{F\rightarrow U}^{H20}$ [22]. With urea as a denaturant, there is sufficient experimental

evidence from the use of the LEM that the m-value of protein unfolding is constant and negative in sign [20-22].

$$\Delta G_{F\rightarrow U} = \Delta G_{F\rightarrow U}^{H20} - m[D] \quad (7)$$

m is the slope of the fitted line, relating the linear change in $\Delta G_{F\rightarrow U}$ to the urea concentration. M-values represent how efficient urea is at unfolding a specific protein/peptide [22,28].

$$m = \frac{\partial \Delta G_{F\rightarrow u}}{\partial [Urea]} \quad (8)$$

Other calculation methods for quantifying denaturant curves include the solvent-exchange model and the denaturant binding model [8,28].

1.5.2. Urea-Induced Unfolding of Alanine-based Monomeric Helical Peptides: Urea Interacts mainly with the Polypeptide Backbone

Scholtz *et al.* (1995) observed that short, alanine-based peptides of defined sequence and length form monomeric helices in aqueous solution with measurable helix contents [24]. Since the helix primarily consist of alanine, side-chain interactions are minimized, limiting how urea interacts with the folded versus unfolded conformations of the peptide [24]. These peptides also lack hydrophobic cores and long-range tertiary interactions. Therefore, any important structural and thermodynamic changes in the unfolding of the peptide should directly result from interactions in the backbone [24].

Far-UV CD monitored the gradual loss of helical structure in all peptides as a function of urea concentration, and the $\Delta G_{F\rightarrow U}$ was determined at each urea concentration for the five peptides [24]. The data was fitted to the linear extrapolation model, which provided an m-value of 23 cal/mol·M per residue [24]. This represents the change in $\Delta G_{F\rightarrow U}$ of a single residue in an α-helix with increase in urea concentration [24]. Table 1 lists the experimental m-values for various globular

proteins possessing different helical contents. To determine the contribution of backbone interactions to helix unfolding, Scholtz *et al.* predicted the m-values for these proteins based on the helix-coil transition m-value (23 cal/mol·M per residue) and the number of α-helical residues present in the protein [24].

Table 1. Comparison between predicted and observed urea m-values of various proteins.

Protein	Protein Data Bank code	No. of residues	No. of helical residues (% helix)	Helix m value[a]	Exp. m value	Helix/Exp. ratio, %
Calbindin D9K	3ICB 75	75	52 (69)	1200	940	128
Trp aporepressor	3WRP	107 (2x)	72 (67)	3310	2900	114
Apomyoglobin (whale)		153	76 (50)	1750	2000	88
Thioredoxin	ITHO	109	48 (44)	1100	1300 1320	85 83
β -Lactamase	3BLM	257	94 (37)	2160	3200[b]	68
RNase A (bovine)	9RSA	124	33 (27)	760	1300 1100 1140 1400 1410	58 69 67 54 54
Dihydrofolate reductase	SDFR	159	43 (27)	990	1900	52
Hen egg-white lysozyme	6LYZ	129	31 (24)	710	1120 1070 1290	63 66 55
Staphylococcal nuclease	2SNS	149	34 (23)	780	2360	33
RNase Ba	1RNB	110	22 (20)	510	1905 1940	27 26
RNase Ti	6NRT	104	17 (16)	390	1210	32
α -Chymotrypsin	4CHA	241	29 (12)	670	2070	32
Chymotrypsinogen A	1CHG	245	17 (7)	390	2030	19

Experimental m-values curated from various studies, referenced and reported by Scholtz *et al.* (1995) [24]. m-values reported in units of cal/mol·M.
a – determined by multiplying the number of helical residues by the m-value for helix unfolded, 23 cal/mol·M. b – deviates from a one-step unfolding system.

As seen in Table 1, proteins with large helical structure content (over 40%) have comparable calculated to experimental m-values, while proteins with a smaller amount of helical structure have larger experimental m-values than the predicted m-values [24]. This means that, as expected, other factors are implicated in the denaturation process which contribute to the m-value [24]. For example, β-sheet unfolding will also contribute to the overall m-value because it leads to the exposure of peptide groups to urea [24]. Nevertheless, the findings of this work do demonstrate that urea is just as efficient in unfolding α-helices as it unfolds globular proteins, indicating that the interaction between urea and peptide groups make up a large part of the denaturation mechanism, and not so much interactions with (hydrophobic) side chains [24].

1.5.3. Free Energy of Transfer of Protein Components from Water to Urea Solutions: Urea Denaturation is driven by Favorable Enthalpic Interactions

To analyze urea's interactions with the peptide groups/backbone and side chains separately, we review thermodynamic studies on three types of model compounds relevant to the protein surface: amino acids (side chain preferences), hydrocarbons (hydrophobic effect), and a polymer resembling the polypeptide backbone (enthalpic interactions with peptide groups). These studies determine the free energy of transfer of the molecules from water to urea solutions, i.e., the difference in ΔG.

Nozaki and Tanford (1963) found that out of the eleven polar and hydrophobic amino acids examined, only the small amino acids glycine and alanine had positive transfer free energies from water to urea solutions (i.e., they do not favorably interact with urea in solution, which causes the $\Delta G_{F \rightarrow U}$ to increase) [25]. These findings indicate that probably the size of the amino acid is an important factor in urea interaction; and that interactions with both polar and hydrophobic side chains are equally significant in the urea unfolding process [25].

The hydrophobic effect is the main stabilizing force of folding in globular proteins. Therefore, it is possible that urea favorably interacts with hydrophobic side chains. Wetlaufer *et al.* (1964) measured transfer free energies of alkane hydrocarbons from water to urea solutions [26]. Hydrocarbons are non-polar and mainly associate through favorable dispersion interactions [26]. It was found that very small hydrocarbons like methane and ethane had positive transfer free energies, while larger hydrocarbons like propane and butane had negative transfer free energies [26]. These results suggest that the hydrophobic effect may be reversed for the larger hydrocarbons in solution in the presence of urea. However, the relative importance of this in the unfolding mechanism has not yet been fully determined [26].

More importantly, the preferential interaction of urea with larger hydrocarbons is a similar observation to what was noticed in the Nozaki and Tanford study on the amino acid side chains. The hydrophobic effect should be similar among hydrophobic solutes irrespective of size, so could the decrease in free energy for the larger hydrocarbons be due to favorable enthalpic interactions (e.g., dispersion interactions) between the solvent and the hydrophobic solutes with larger surface area? Could this also be the case for the larger amino acid side chains? A decrease in both the entropy and enthalpy of transfer was observed in the hydrocarbon-urea system when considering the energetic effects of solvent H-bonding restructuring [26]. This means that the decrease in enthalpy must be the driving force for the decrease in transfer free energy, per Eq-6.

Robinson and Jencks (1965) also performed transfer free energy studies on a model polar biopolymer which resembles the polypeptide backbone in proteins. The free energy, enthalpy, and entropy of transfer from water to urea were all found to be negative for this polar compound [27]. This also indicates that enthalpy is the driving force for the negative transfer free energy. However,

it is important to note that the likeness of urea's structure to the peptide bond could be the facilitator of this interaction [27].

In general, these results show that urea addition increases the solubility of the hydrophobic and amide moieties in aqueous solvent [25-27]. The interactions responsible for denaturation may decrease the enthalpy and entropy of the protein-solvent system, but the decrease in enthalpy is the major driving force for unfolding, as it directly decreases the Gibbs free energy (i.e., stability) of the protein [25-27]. These deductions indicate that the reversal of the hydrophobic effect in urea solutions may not be spontaneous, and it may just occur as a result of the enthalpy-driven unfolding process [25-27].

1.6. Proposed Mechanisms of Urea Denaturation: Experimental Findings & Insights into Theoretical Models

It is possible that urea may interact with proteins directly (urea-protein interaction) and/or indirectly (urea-solvent interaction) through a combination of one or more of the following simply explained denaturation models [6, 27-47]:

Direct:

(i) **Denaturant binding model:** Urea competes with water for specific binding (H-bonding, dispersion interactions) with the polypeptide backbone and/or side chains. The binding sites increase as more surface area of the protein is exposed with unfolding [27-34, 43-47].

(ii) **Solvent-exchange model:** Urea's preferential interaction with the polypeptide backbone excludes water. There is therefore an equilibrium of water to urea binding sites on the protein [28,30].

Indirect:

(i) **Urea alters water structure**: Urea is thought to disrupt the H-bonding network between water molecules. This in turn reduces the ordering of water molecules around the hydrophobic side chains, enhancing their solvation and decreasing the net hydrophobic effect [35,36,37,54-56].

The indirect mechanism does not agree well with what is presently known about urea. The free energy of transfer and monomeric peptide analyses show that urea addition to aqueous solvent increases the solubility of the protein surface (mainly the backbone, also the side chains) through an enthalpy-driven process, and this increase in solubility is the cause of unfolding [24-27]. The indirect model implies that urea acts through reversal of the hydrophobic effect, which has already shown to be an unlikely driving mechanism for unfolding. Although a number of computational studies suggest that the indirect mechanism may (at least partially) contribute to the denaturing properties of urea, conclusive experimental evidence for this mechanism has not yet materialized [35,36,37]. An X-ray diffraction study by Sahle *et al.* (2016) shows a weak interaction between urea and water, implying that urea does not largely alter water structure [39]. Hayashi *et al.* (2007) also showed through dielectric spectroscopy measurements of aqueous urea solutions that urea hardly perturbs the H-bonding network of water [40].

Moreover, urea is a small, polar molecule that readily incorporates into water at high molar concentrations (up to 9 M), forming H-bonds with both the amine and carbonyl headgroups. If it were to significantly alter water structure, this would not be energetically possible [15,57,58]. Though it is plausible that urea does exert some changes to the overall H-bonding network, it is likely a cooperative effect (i.e., H-bonds between urea-water, water-water, and urea-urea are similar and interchangeable) [5-8,15]. It is therefore reasonable to assume that urea meshes well into the H-

bonding network of water without disrupting its spatial distribution, in marked contrast to water-methanol systems [5,39,40]. Neutron scattering data also demonstrate that urea addition causes a reduction in the void volume of the solvent, but this structural change should cause a reduction in hydrocarbon solubility, not an increase [38,41,59-61]. Lastly; the urea-protein interaction is very weak, given that high molar amounts are needed for destabilization of most proteins [5-8]. It would make more sense that urea directly contacts proteins in solution.

The direct mechanism of urea action is gradually gaining traction among protein folding researchers [62-67]. The main question is, what is the nature of the interaction? Originally, it was thought that urea unfolds proteins mainly through strong electrostatic H-bonding interactions with amide groups and other polar moieties that can preferentially solvate, and thus increase the solubility of the amide backbone in water [27,32,33]. Experimental data appear to be less conclusive about urea's denaturation mechanism: NMR studies by Lim *et al.* (2009) have shown that urea can interact both as a H-bond donor and H-bond acceptor with model peptide compounds [44]. Meanwhile, Fourier-transform infrared spectroscopy data by Sagle *et al.* (2009) show that from the solute perspective, substituting water molecules with urea either has a small effect upon the H-bond donating properties of aqueous solvent, or slightly reduces its H-bond donation capabilities [45,68,69]. These findings are inconsistent with a H-bonding driven mechanism of urea unfolding.

Though it is understood that urea mainly interacts with the polypeptide backbone, H-bonding interactions with the protein surface cannot fully explain the enhanced solvation of the hydrophobic side chains of larger, globular proteins in urea-water solutions. Since the unfolding of globular proteins leads to the exposure of the side chains (mainly hydrophobic) to the solvent, urea must be able to interact favorably with both hydrophobic and polar side chains. Dispersion interactions are weak, short-range, electrostatic forces that attract neutral molecules to one another

through dipole-induced dipole interactions [10]. Dispersion interactions are not as discriminating as electrostatic interactions with regards to polarity [2,19]. Computational work by Stumpe *et al.* (2008) shows that hyperpolar urea in solution exhibits increased denaturation power, while hypopolar urea stabilizes the native state of proteins more [46]. These results strongly suggest that apolar urea–protein interactions are the main driving force in denaturation [46]. More recent theoretical work also suggests that H-bonding of urea to the protein backbone plays a minor role in the denaturation process, and it is mainly van der Waals interactions between urea and protein moieties that cause denaturation [70,71].

The computational analyses of Hua *et al.* indicate that direct van der Waals dispersion interactions between urea and the protein surface (backbone and side chains) are stronger than that of water, leading them to suggest that urea-induces protein unfolding through the following 2-step process: first, urea displaces water molecules in the first solvation shell of the protein which allows it to then bind tighter to the protein surface both through more favorable dispersion interactions and acting as a strong H-bond acceptor (via its carbonyl oxygen). Subsequently urea and water can solvate the exposed hydrophobic, polar, and charged residues [47]. Clearly, more experimental evidence is required in order to confirm or rule out the suggested mechanisms above.

1.7. Aim of the Project: Experimental Investigation of the Mechanism of Action of Urea

In this work, we will attempt to answer the following three questions through studying how urea affects the solvation properties of six judiciously selected model compounds (Fig. 2). First, does urea addition significantly change the H-bonding acceptor properties of the aqueous solvent? Second, can the presence of urea disrupt or weaken intramolecular H-bonds? Third, can the increase in amide solubility seen in water-urea binary mixtures be unambiguously assigned to favorable van der Waals interactions between urea and the solute rather than H-bonding? The next chapters of this thesis provide a detailed synopsis of how we studied the three model systems, the results from these experiments, and a final discussion of our findings.

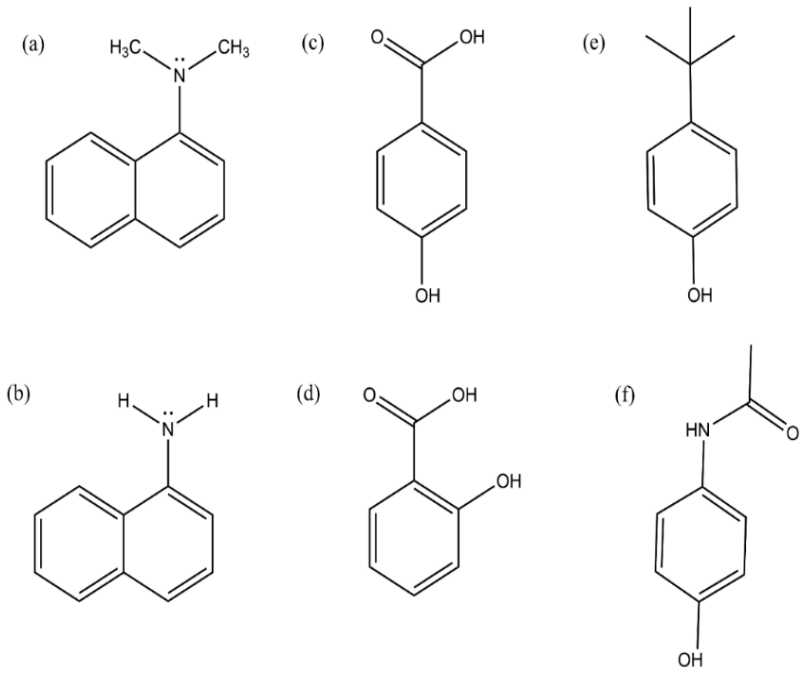

Figure 2. Model compounds used in this study: (a) 1-dimethyalminonaphthalene (b)1-aminonapthalene (c) *para*-hydroxybenzoic acid (d) *ortho*-hydroxybenzoic acid (e) 4-tertbutylphenol (f) acetaminophen.

References:

1. Dill, K.A., Ozkan, S.B., Shell, M.S., Weikl, T.R. The protein folding problem. *Annual Review of Biophysics*. (2008); 37, 289-316.
2. Pace, N., Scholtz, C., Martin, J., Grimsley, G. R. Forces stabilizing proteins. *FEBS Letters*. (2014); 588(14), 2177-84.
3. Baldwin, R. L. Energetics of protein folding. *Journal of Molecular Biology*. (2007); 371 (2), 283–301.
4. Walters, J., Milam, S.L., Clark, A.C. Practical approaches to protein folding and assembly: spectroscopic strategies in thermodynamics and kinetics. *Methods in Enzymology*. (2009); 455, 1-39.
5. Canchi, D.R., García, A.E. Co-solvent effects on protein stability. *Annual Review of Physical Chemistry.* (2013); 64, 273-93.
6. England, J.L., Haran, G. Role of solvation effects in protein denaturation: from thermodynamics to single molecules and back. *Annual Review of Physical Chemistry.* (2011); 62, 257-277.
7. Schellman, J. A. Solvent denaturation. *Biopolymers*. (1978); 17 (5), 1305–1322.
8. Tanford, C. Protein denaturation. *Advances in Protein Chemistry.* (1968); 23, 121– 282.
9. Santra, M., Dill, K.A., de Graff A.M.R. How do chaperones protect a cell's proteins from oxidative damage? *Cell Systems.* (2018); 6(6), 743-751.
10. Dill, K.A. Dominant forces in protein folding. *Biochemistry.* (1990); 29, 7133–7155.
11. Pace, C.N., Scholtz, J.M. Measuring the conformational stability of a protein. Protein structure: a practical approach. *Methods in Molecular Biology.* (1997); (168), 299-321.

12. Fitter, J. A measure of conformational entropy change during thermal protein unfolding using neutron spectroscopy. *Biophysical Journal*. (2003); 84(6), 3924-3930.

13. Baldwin, R. L., Rose, G. D. How the hydrophobic factor drives protein folding. *Proceedings of the National Academy of Sciences of the United States of America*. (2016); 113 (44), 12462–12466.

14. Kuznetsova, I.M., Zaslavsky, B.Y., Breydo, L., Turoverov, K.K., Uversky, V.N. Beyond the excluded volume effects: mechanistic complexity of the crowded milieu. *Molecules*. (2015); 20(1), 1377-1409.

15. Rösgen, J., Pettitt, B.M., Bolen, D.W. Protein folding, stability, and solvation structure in osmolyte solutions. *Biophysical Journal.* (2005); (89)5, 2988 – 2997.

16. Mojtabavi, S., Samadi, N., Faramarzi, M.A. Osmolyte-induced folding and stability of proteins: concepts and characterization. *Iran Journal of Pharmaceutical Research*. (2019); 18, 13-30.

17. Van der Vegt, N. F. A., Nayar, D. The hydrophobic effect and the role of co-solvents. *The Journal of Physical Chemistry B*. (2017); 121 (43), 9986–9998.

18. Schellman, J. A. Protein stability in mixed solvents: a balance of contact interaction and excluded volume. *Biophysical Journal.* (2003); 85 (1), 108–125.

19. Brooks, C. L., Nilsson, L. Promotion of helix formation in peptides dissolved in alcohol and water-alcohol mixtures. *Journal of the American Chemical Society*. (1993); 115(23), 11034–11035.

20. Santoro M.M, Bolen D.W. Unfolding free energy changes determined by the linear extrapolation method. Unfolding of phenylmethanesulfonyl alpha-chymotrypsin using different denaturants. *Biochemistry.* (1988); 27(21), 8063-8068.

21. Greene, J., Pace, C. N. Urea and guanidine hydrochloride denaturation of ribonuclease, lysozyme, alpha-chymotrypsin, and beta-lactoglobulin. *The Journal of Biological Chemistry*. (1974); 249 (17), 5388–5393.

22. Pace, C. N., Shaw, K. L. Linear extrapolation method of analyzing solvent denaturation curves. *Proteins, Structure, Function, and Bioinformatics*. (2000); 41(S4), 1–7.

23. Amsdr, A., Noudeh, N.D., Liu L., Chalikian, T.V. On urea and temperature dependences of m-values. *The Journal of Chemical Physics*. (2019); 150 (21), 215103–215103.

24. Scholtz, J. M., Barrick, D., York, E. J., Stewart, J. M., Baldwin, R. L. Urea unfolding of peptide helices as a model for interpreting protein unfolding. *Proceedings of the National Academy of Sciences of the United States of America.* (1995); 92(1), 185-189.

25. Nozaki, Y., Tanford, C. The solubility of amino acids and related compounds in aqueous urea solutions. *The Journal of Biological Chemistry*. (1963); 238, 4074–4081.

26. Wetlaufer, D. B., Malik, S. K., Stoller, L., Coffin, R. L. Nonpolar group participation in the denaturation of proteins by urea and guanidinium salts. Model compound studies. *Journal of the American Chemical Society.* (1964); 86, 508–514.

27. Robinson, D. R., Jencks, W. P. The effect of the urea- guanidinium class on the activity coefficient of acetyltetraglycine ethyl ester and related compounds. *Journal of the American Chemical Society.* (1965); 87, 2462–2470.

28. Tanford, C. Protein denaturation: Theoretical models for the mechanism of denaturation. *Advances in Protein Chemistry.* (1970); 24, 1–95.

29. Wu, J.W., Wang Z.X. New evidence for the denaturant binding model. *Protein Science*. 1999; 8(10), 2090-2097.

30. Wu, H. Studies on denaturation of proteins XIII. A theory of denaturation. *Chinese Journal of Physiology*. (1931); V(4), 321–344.

31. Street, T.O., Bolen, D.W., Rose, G.D. A molecular mechanism for osmolyte-induced protein stability. *Proceedings of the National Academy of Sciences of the United States of America.* (2006); 103:13997–14002.

32. Tobi, D., Elber, R., Thirumalai, D. The dominant interaction between peptide and urea is electrostatic in nature: A molecular dynamics simulation study. *Biopolymers.* (2003); 68:359–369.

33. O'Brien, E.P., Dima, R.I., Brooks, B., Thirumalai, D. Interactions between hydrophobic and ionic solutes in aqueous guanidinium chloride and urea solutions: Lessons for protein denaturation mechanism. *Journal of the American Chemical Society.* (2007);129:7346–7353.

34. Canchi, D. R., García, A. E. Backbone and side-chain contributions in protein denaturation by urea. *Biophysical Journal*. (2011); 100 (6), 1526–1533.

35. Bennion, B.J., and V. Daggett, V. The molecular basis for the chemical denaturation of proteins by urea. *Proceedings of the National Academy of Sciences of the United States of America*. (2003); 100, 5142–5147.

36. Stumpe, M. C., Grubmüller, H. Interaction of urea with amino acids: implications for urea-induced protein denaturation. *Journal of the American Chemical Society*. (2007); 129 (51), 16126–16131.

37. Das, A., Mukhopadhyay, C. Urea-mediated protein denaturation: a consensus view. *The Journal of Physical Chemistry B*. (2009);113:12816–12824.

38. Soper, A. K., Castner, E. W. Luzar, A. Impact of urea on water structure: A clue to its properties as a denaturant? *Biophysical Chemistry,* (2003); 105, 649–666.

39. Sahle, C.J., Schroer, M.A, Juurinen, I., Niskanen, J. Influence of TMAO and urea on the structure of water studied by inelastic X-ray scattering. *Physical Chemistry Chemical Physics: PCCP*. (2016); 18(24), 16518-16526.

40. Hayashi, Y., Katsumoto, Y., Omori, S., Kishii, N., Yasuda, A. Liquid structure of the urea-water system studied by dielectric spectroscopy. *The Journal of Physical Chemistry.* (2007); 111(5), 1076–1080.

41. Burton, R.C., Ferrari, E.S., Davey, R. J., Hopwood, J., Quayle, M.J., Finney, J.L., Bowron, D.T. The structure of a supersaturated solution: A neutron scattering study of aqueous urea. *Crystal growth & design*. (2008); 8 (5), 1559–1565.

42. Prakash, V., Loucheux, C., Scheufele, S., Gorbunoff, M.J., Timasheff, S.N. Interactions of proteins with solvent components in 8 M urea. *Archives of Biochemistry and Biophysics.* (1981); 210(2):455-64.

43. Almarza, J., Rincon, L., Bahsas, A., Brito, F. Molecular mechanism for the denaturation of proteins by urea. *Biochemistry*. (2009);48 (32), 7608–7613.

44. Lim, W.K., Rösgen, J., Englander, S.W. Urea, but not guanidinium, destabilizes proteins by forming hydrogen bonds to the peptide group. *Proceedings of the National Academy of Sciences of the United States of America*. (2009); 106(8), 2595-2600.

45. Sagle, L. B., Zhang, Y., Litosh, V. A., Chen, X., Cho, Y., Cremer, P. S. Investigating the hydrogen-bonding model of urea denaturation. *Journal of the American Chemical Society.* (2009); 131(26), 9304–9310.

46. Stumpe, M. C., Grubmüller, H. Polar or Apolar—The Role of polarity for urea-induced protein denaturation. *PLOS Computational Biology*. (2008);4(11): e1000221.

47. Hua, L. Urea denaturation by stronger dispersion interactions with proteins than water implies a 2-Stage unfolding. *Proceedings of the National Academy of Sciences of the United States of America*. (2008); 105 (44), 16928–16933.

48. Lapidus, L. J. Protein unfolding mechanisms and their effects on folding experiments. *F1000Research. (*2017); *6*, 1723.

49. Canchi, D. R., Paschek, D., García, A. E. Equilibrium study of protein denaturation by urea. *Journal of the American Chemical Society.* (2010); *132* (7), 2338-2344.

50. Auton, M., Holthauzen, L. M. F., Bolen, D. W. Anatomy of energetic changes accompanying urea-induced protein denaturation. *Proceedings of the National Academy of Sciences.* (2007); *104* (39), 15317-15322.

51. Guinn, E. J., Pegram, L. M., Capp, M. W., Pollock, M. N., Record, M. T., Jr. Quantifying why urea is a protein denaturant, whereas glycine betaine is a protein stabilizer. *Proceedings of the National Academy of Sciences.* (2011); *108* (41), 16932-7.

52. Cheng, X., Shkel, I. A., O'Connor, K., Henrich, J., Molzahn, C., Lambert, D., Record, M. T. Experimental atom-by-atom dissection of amide–amide and amide–hydrocarbon Interactions in H_2O. *Journal of the American Chemical Society.* (2017); *139* (29), 9885-9894.

53. Auton, M., Bolen, D. W., Chapter Twenty-Three - Application of the transfer model to understand how naturally occurring osmolytes affect protein stability. In *Methods in Enzymology*, Häussinger, D.; Sies, H., Eds. Academic Press: (2007); Vol. 428, pp 397-418.

54. Frank, H. S., Evans, M. W., Free volume and entropy in condensed systems III. Entropy in binary liquid mixtures; partial molal entropy in dilute solutions; structure and thermodynamics in aqueous electrolytes. *Journal of Chemical Physics.* (1945); *13*, 507-532.

55. Frank, H. S., Franks, F., Structural approach to solvent power of water for hydrocarbons - urea as a structure breaker. *Journal of Chemical Physics.* (1968); *48* (10), 4746.

56. Hoccart, X., Turrell, G., Raman-spectroscopic investigation of the dynamics of urea-water complexes. *Journal of Chemical Physics.* (1993); *99* (11), 8498-8503.

57. Sharp, K. A., Madan, B., Manas, E., Vanderkooi, J. M., Water structure changes induced by hydrophobic and polar solutes revealed by simulations and infrared spectroscopy. *The Journal of Chemical Physics.* (2001); *114* (4), 1791-1796.

58. Rezus, Y. L. A., Bakker, H. J., Effect of urea on the structural dynamics of water. *Proceedings of the National Academy of Sciences.* (2006); *103* (49), 18417-18420.

59. Shoor, S. K., Gubbins, K. E., Solubility of nonpolar gases in concentrated electrolyte solutions. *The Journal of Physical Chemistry.* (1969); *73* (3), 498-505.

60. Masterton, W. L., Lee, T. P., Salting coefficients from scaled particle theory. *The Journal of Physical Chemistry.* (1970); *74* (8), 1776-82.

61. Graziano, G. On the Solubility of Aliphatic Hydrocarbons in 7 M Aqueous Urea. *The Journal of Physical Chemistry.* (2001); *105* (13), 2632-2637.

62. Berteotti, A., Barducci, A., Parrinello, M. Effect of Urea on the β-Hairpin Conformational Ensemble and Protein Denaturation Mechanism. *Journal of the American Chemical Society.* (2011); *133* (43), 17200-17206.

63. Yang, Z., Xiu, P., Shi, B., Hua, L., Zhou, R. Coherent Microscopic Picture for Urea-Induced Denaturation of Proteins. *The Journal of Physical Chemistry B.* (2012); *116* (30), 8856-8862.

64. Bolen, D. W., Rose, G. D. Structure and Energetics of the Hydrogen-Bonded Backbone in Protein Folding. *Annual Review of Biochemistry.* (2008); *77* (1), 339-362.

65. Jha, S. K., Marqusee, S. Kinetic evidence for a two-stage mechanism of protein denaturation by guanidinium chloride. *Proceedings of the National Academy of Sciences.* (2014); *111* (13), 4856-4861.

66. Ganguly, P., Shea, J.-E. Distinct and Nonadditive Effects of Urea and Guanidinium Chloride on Peptide Solvation. *The Journal of Physical Chemistry Letters.* (2019); *10* (23), 7406-7413.

67. Garidel, P., Eiperle, A., Blech, M., Seelig, J. Thermal and Chemical Unfolding of a Monoclonal IgG1 Antibody: Application of the Multistate Zimm-Bragg Theory. *Biophyics Journal.* (2020); *118* (5), 1067-1075.

68. Ding, B., Yang, L., Mukherjee, D., Chen, J., Gao, Y., Gai, F. Microscopic Insight into the Protein Denaturation Action of Urea and Its Methyl Derivatives. *The Journal of Physical Chemistry Letters.* (2018); *9* (11), 2933-2940.

69. Pazos, I. M., Gai, F. Solute's Perspective on How Trimethylamine Oxide, Urea, and Guanidine Hydrochloride Affect Water's Hydrogen Bonding Ability. *The Journal of Physical Chemistry B.* (2012); *116* (41), 12473-12478.

70. Li, W., Zhou, R., Mu, Y. Salting effects on protein components in aqueous NaCl and urea solutions: Toward understanding of urea-induced protein denaturation. *The Journal of Physical Chemistry B.* (2012); *116* (4), 1446-1451.

71. Zangi, R., Hagen, M., Berne, B. J. Effect of ions on the hydrophobic interaction between two plates. *Journal of the American Chemical Society*. (2007); *129* (15), 4678-4686.

Chapter 2.

Materials & Methods

2.1. Materials

1-aminonapthalene, 1-dimethylaminonapthalene, acetaminophen, tert-butylphenol, hexane, cyclohexane, chloroheptane, chlorohexane, dichloromethane, dichloroethane, dibutyl ether, diethyl ether, ethyl acetate, acetonitrile, methanol, ethanol, propanol, ethylene glycol, activated charcoal, sodium formate, formic acid, sodium hydroxide, deuterium oxide and potassium fluoride were purchased from Sigma Aldrich (Burlington, MA). Trimethylamine-N-oxide, urea, *ortho*-hydroxybenzoic acid and *para*- hydroxybenzoic acid were purchased from ThermoFisher Scientific (Fairlawn, NJ). All materials were purchased at highest commercial purity.

2.2. Methods

2.2.1. Fluorescence Spectroscopy

Fluorescence spectroscopy is a sensitive technique used to characterize and detect structural changes in various kinds of molecules due to changes in microenvironment [72]. The intensity of photons emitted by a fluorescent molecule in solution following photoexcitation may be detected as a function of wavelength using a spectrofluorometer [73,74].

The spectrofluorometer consists of the following parts: a constant source of light for excitation (typically a xenon-based lamp), a monochromator to select the emission and excitation wavelengths, entrance and exit slits for the light source and the detector respectively, shutters to eliminate interfering light from both channels, a light beam splitter which is used to provide a reference reading before the light meets the sample, a sample holder for the cuvette, and a detector (usually a photomultiplier tube) [72-74].

The fluorescence intensity is measured using a specialized computer software which converts the reading into a spectrum. Emission spectra measures the fluorescence of molecules at a fixed excitation wavelength, and a range of wavelengths of lower energy are scanned to detect photon emission [74]. Figure 3(a) represents a schematic illustration of a spectrofluorometer, and Fig. 3(b) shows the actual spectrofluorometer used in this work.

(a)

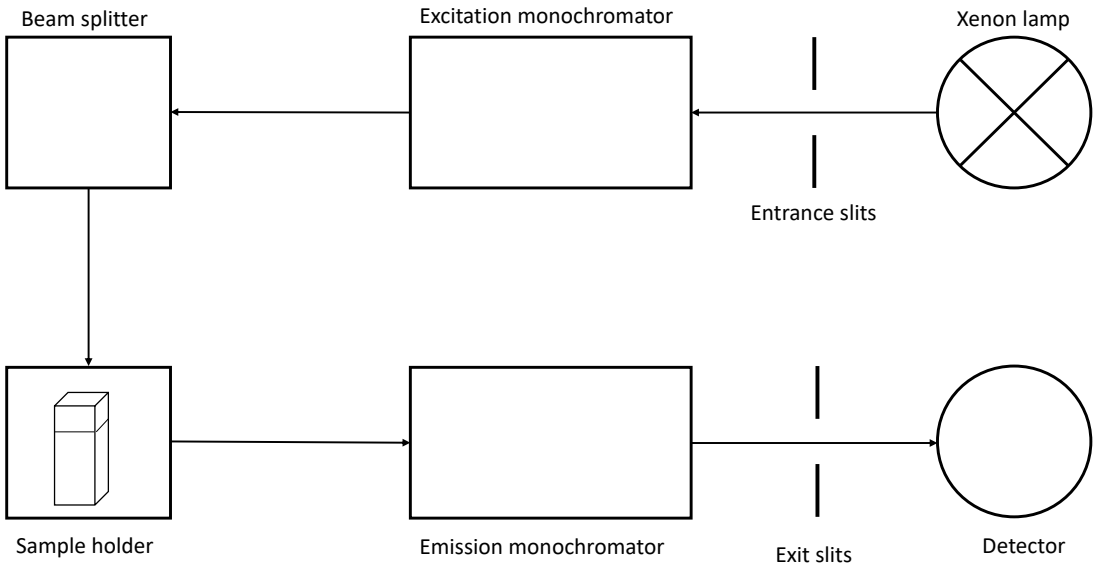

(b)

Figure 3. (a) schematic diagram of the typical constituents of a spectrofluorometer. (b) Fluorolog-3 Horiba Jobin Yvon Spectrofluorometer.

2.2.2. UV/Vis Absorbance Spectroscopy

Absorbance spectroscopy is a technique used to measure the absorption of light energy in the UV-Visible region by a specific substance [75]. The intensity of light absorbed at different wavelengths varies between molecules, so it is a very useful technique for the identification and quantitative determination of a substance of interest. The instrument used in this work is a double-beam spectrophotometer, its working principle is described below and depicted in Fig. 4.

The spectrophotometer consists of a light source, which is usually a combination of two lamps: a deuterium lamp used for the UV part of the spectrum, and a tungsten/halogen lamp for the visible part. The output of the two bulbs combined is focused onto a diffraction grating which splits the incoming light into its constituent colours, followed by a slit which allows light of a selected range of wavelengths to pass through to the rest of the instrument. This beam of light hits the rotating disc and is split into two beams; one beam interacts with the sample cell, while the other simultaneously interacts with the reference cell [75,76].

The incoming light beams encounter the another rotating disc and then enter the detector which measures the light intensity transmitted from the sample, (I) compared to the intensity of light transmitted from the reference cell (I_0) [72-76]. The transmittance, T of the sample is the ratio of I to I_0, Absorbance is a dimensionless quantity related to transmittance that is obtained from the spectrophotometer as a function of wavelength (absorption spectra). Beer-Lamber's Law allows us to accurately determine the concentration of a molecule in solution using the following equation [72-76]:

$$-Log(T) = A = \varepsilon lc \qquad (9)$$

Where A is the absorbance measured, is the molar absorptivity coefficient, l is the pathlength of the cuvette (cm), and c is the concentration of the molecule.

(a)

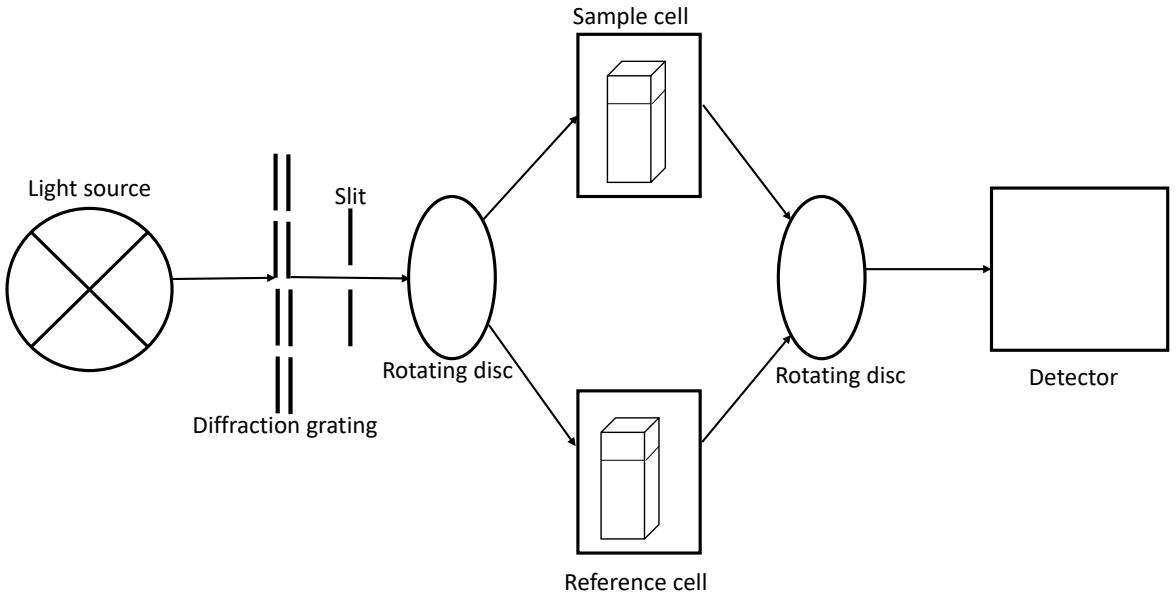

(b)

Figure 4. (a) schematic diagram of the basic components of a double-beam UV-Vis spectrophotometer. (b) Agilent Cary 5000 UV-Vis-NIR spectrophotometer.

2.2.3. pH Determination with Fluorine NMR Spectroscopy

Fluorine nuclear magnetic resonance (Fluorine NMR) spectroscopy is a highly sensitive technique which exploits the broad chemical shift range and large chemical shift response of the ^{19}F nucleus to the local environment [77,78]. Protonation of the fluoride ion (F^-) perturbs the chemical shift (δ) of ^{19}F nuclei, and the ratio of hydrofluoric acid to fluoride ion $\frac{[F^-]}{[HF]}$ in a solution can be determined by measuring changes in δ, represented by the following equation [78]:

$$\frac{[F^-]}{[HF]} = \left(\frac{\delta_{F-} - \delta_{obs}}{\delta_{obs} - \delta_{HF}}\right) \quad (10)$$

Where δ_{F^-} is the chemical shift of the fully deprotonated F^- (pH 7) in solution, δ_{HF} is the chemical shift of the full protonated HF (pH 1) in solution, and δ_{obs} is the chemical shift of the solution of interest. This method has been exploited by Gerken *et al.* (2010) to measure the pK_a of fluoride by plotting the measured $\frac{[F^-]}{[HF]}$ against potentiometric pH titration curves, according to the Henderson Hasselbach equation [78]:

$$pH = pK_a + \frac{[F^-]}{[HF]} \quad (11)$$

Conversely, fluoride ion and fluoride-containing compounds of known pK_a can be used as pH indicators/probes of their solution environment, where their chemical shifts are used to detect and measure changes in the ratios of the protonated to unprotonated form of the probe (determined from δ) present in the solution [78]. After Hydrogen fluoride (HF), potassium fluoride (KF) is the primary source of fluoride ion used in fluorine NMR experiments. In this work, the F^-/HF system was used as an pH probe in the spectrophotometric titration of hydroxybenzoic acids (HBAs) in binary co-solvent-water mixtures.

2.2.4. Preparation of Binary Solvent Mixtures

Required urea-water binary mixtures were prepared at nominal concentration and the refractive index of the resulting solution was determined using an Abbe refractometer purchased from ThermoFisher Scientific (Fairlawn, NJ). The true urea concentration was determined using the equation: [Urea] = $117.66(\Delta\eta) + 29.753(\Delta\eta)^2 + 185.56(\Delta\eta)$[51]. Methanol-water and acetonitrile-water mixtures were prepared by weight, their density determined using a pycnometer, and their concentrations determined using literature values[79,80].

2.2.5. Fluorescence of 1-AN and 1-DMAN

The fluorescence spectra of 1-AN and 1-DMAN in various solvents were measured at room temperature (20 °C) using a Fluorolog-3 Horiba Jobin Yvon Spectrofluorometer (Edison, NJ) and quartz cuvettes of 1×1/3 cm path length. Entrance and exit slits were set to 2 nm bandpass resolution. In order to prevent solute aggregation and non-linear effects the concentration of each sample was adjusted until the optical density was below 0.1 and a fluorescence intensity between 100,000-900,000 counts was obtained for the emission spectra maxima. The fluorescence emission maxima peaks were fitted to a Weibull 5 parameter distribution equation using SigmaPlot (Palo Alto, CA) data analysis software for accurate emission peak wavelength determination.

2.2.6. Spectroscopic Determination of *ortho*- and *para*-hydroxybenzoic acid pKa Values

(a) *o*-HBA and *p*-HBA sample preparation

Solutions of 100 μM *o*-HBA and 25 μM *p*-HBA were prepared volumetrically in the solvent of choice, solutions were buffered using 50 mM sodium formate and the pH was adjusted nominally using 98% formic acid and a pH meter, enough potassium fluoride was added to ensure

a final formal concentration of 2 mM to function as an NMR probe. The samples were left to equilibrate for 1 hour at room temperature in the dark before the spectroscopic readings, F-NMR and absorbance measurements for each sample were done in tandem.

(b) Fluorine-NMR measurements

Potassium fluoride was used as an F-NMR probe to determine the pH of fluoride containing samples[77,78]. At any given pH the total concentration of fluoride ion plus hydrogen fluoride was kept constant at 2 mM and enough deuterium oxide was added to buffer to obtain approximately 10 percent by volume D_2O/H_2O. With the help of Dr. Dave Davidson, ^{19}F-NMR spectra with 1H-decoupling were recorded at a frequency of 282.376 MHz on a Bruker Avance DRX 300 MHz NMR spectrometer equipped with a 5 mm QNP probe (1H/13C/19F/31P). Spectra were averaged over 128 scans at room temperature with a spectral width of 67.5 kHz, utilizing 131072 data points for acquisition in a time of 1s, relaxation delay 1s, using Waltz-16 proton decoupling. All spectra were processed using Bruker Topspin software by Dr. Dave Davidson. Prior to Fourier transformation all time domain data was processed with an exponential window function using a line broadening of 5 Hz. ^{19}F resonances were referenced relative to lock solvent (10 percent by volume D_2O/H_2O). For all measurements the chemical shifts measured at pH 1 and pH 7 are assumed to be respectively, the characteristic shifts of aqueous hydrogen fluoride and fluoride anion.

(c) Determination of the concentrations of acidic and basic forms of *o*-HBA and *p*-HBA

UV absorbance spectra were measured at room temperature (20 ^{o}C) using an Agilent Cary 5000 UV-Vis-NIR spectrophotometer (Santa Clara, CA) and quartz cuvettes having 1×1 cm path

length. The spectra were collected between 220 to 330 nm with a scan rate of 60 nm/min. A working isosbestic point for the acidic/basic forms of each isomer (300 nm for *o*-HBA, 247 nm for *p*-HBA) was determined through observing the pH dependent evolution of the spectrum of each compound (see Fig. S3). In order to determine $\frac{[A^-]}{[HA]}$, the absorbance of each *o*-HBA sample was determined at 310 nm and 300 nm, while that of *p*-HBA was determined at 261nm and 247 nm. In order to account for small variations in sample concentration, all measured absorbance values are normalized to absorbance values measured at their relevant isosbestic point. The ratio $\frac{[A^-]}{[HA]} = (\frac{A_{obs}-A_{acid}}{A_{basic}-A_{acid}})$ is determined using: A_{obs} the normalized absorbance of a given sample measured at 310 nm for o-HBA and 261 nm for *p*-HBA, A_{acid} the normalized absorbance of the acidic form (at pH 1) measured at 310 nm for *o*-HBA and 261 nm for *p*-HBA, and A_{basic} the normalized absorbance of the basic form (at pH 7) measured at 310 nm for *o*-HBA and 261 nm for *p*-HBA.

2.2.7. Spectrophotometric Determination of Acetaminophen and 4-tertbutylphenol Solubilities

(a) Determination of the extinction coefficients of acetaminophen and 4-tertbutylphenol

In order to determine the molar absorptivity (extinction coefficient), we quantitatively transferred 0.035g of 4-tertbutylphenol and 0.035 g of acetaminophen in separate 10 ml volumetric flasks in order to obtain a 2.31mM stock solution of acetaminophen and 2.33 mM stock solution of 4-tertbutylphenol. Each stock was used to make solutions having an appropriate concentration of analyte by volumetric dilution in water. All absorbance measurements were done using an Agilent Cary 5000 UV-Vis-NIR spectrophotometer and a semi-micro quartz cuvette of 1×1/3 cm pathlength.

(b) Measurement of the solubility of acetaminophen and 4-tertbutylphenol in binary mixtures of urea-water and acetonitrile-water

In order to determine the solubilities of acetaminophen and 4-tertbutylphenol in a given solvent system, 5 mL of a given solvent was mixed with an excess solid amount of either acetaminophen or 4-tertbutylphenol (~ 5-10 mg) in screw-capped vials and shaken vigorously by vortexing for 30 seconds. Afterwards, each sample was heated to 45 °C in a temperature-controlled water bath, kept at 45 °C for 10 minutes and then left to cool to room temperature (20 °C) for 4-6 hours in the dark, in order to reach equilibrium. The samples were then filtered with 0.2-micron syringe filter to separate the saturated supernatant from the solid particulate matter. The filtrate was then diluted volumetrically by a factor of 1000 for acetaminophen and by a factor of 50 for 4-tertbutylphenol in pure water and the concentration of the resulting solution was determined by absorbance using an extinction coefficient of 3240±95 at 260 nm for acetaminophen and 1520 ±25 at 275 nm for 4-tertbutylphenol (see Section 3.3.4). The original sample concentration was calculated using the appropriate dilution factor.

References:

72. Lakowicz, J.R. Principles of fluorescence spectroscopy. *Springer* (2006).
73. Eftink M.R. The use of fluorescence methods to monitor unfolding transitions in proteins. *Biophysics Journal.* (1994); 66, 482–501.
74. Guilbault, G.G. Fluorescence, theory, instrumentation and practice. Marcel Dekker Inc. (1967).
75. Wormell, P., Rodger, A. Absorbance Spectroscopy: Overview. Encyclopedia of Biophysics. Springer, Berlin, Heidelberg. (2013); pp 23-25.
76. Ewing, G.W. Instrumental methods of chemical analysis, 3rd Edition. McGraw-Hill Book Co. (1969).
77. Gerig, J.T. Fluorine nuclear magnetic resonance of fluorinated ligands. Methods in Enzymology. (1989);177:3-23.
78. Gerken J.B. Measurement of pH by NMR Spectroscopy in concentrated aqueous fluoride buffers. *Journal of Fluorine Chemistry*. (2011); 132(1), 68-70.
79. Mikhail, S. Z., Kimel, W. R. Densities and Viscosities of Methanol-Water Mixtures. *Journal of Chemical & Engineering Data.* (1961); *6* (4), 533-537.
80. Cunningham, G.P., Vidulich, G.A., Kay, R.L. Several properties of acetonitrile-water, acetonitrile-methanol, and ethylene carbonate-water systems. *Journal of Chemical & Engineering Data* (1967); *12* (3), 336-337.

Chapter 3.

Results & Discussion

Part I: Determination of the Effects of Urea Addition on H-bonding Donor/Acceptor Properties of Aqueous Solvent Systems

3.1.1. Solvatochromism of Aminonapthalenes

In order to understand how urea affects the H-bonding donor/acceptor properties of aqueous solvent, we measure how its addition affects the fluorescent solvatochromic shifts of aminonaphthalenes (ANs). ANs are strong electron donors that form highly polar excited states following photoexcitation of the naphthalene moiety [81-84]. The electronic spectra of ANs are dependent on both solvent polarity (dipole-dipole interactions) and H-bond donation/acceptance [82,83]. They therefore can act as highly-sensitive probes to detect slight changes in solvent properties.

1-aminonaphthalene (1-AN) and 1-dimethylaminonaphthalene (1-DMAN) have similar ground and excited state dipole moments, as well as having only one lone-pair of electrons in similar geometry functioning as a H-bond acceptors, as seen in Fig. 5 [81-83]. However, the amine hydrogens of 1-AN can also interact with solvent through H-bond donation, which further stabilizes 1-AN in H-bond acceptor solvents [83]. Comparing fluorescence solvatochromic shifts of 1-AN with 1-DMAN makes it possible to highlight the contribution of solvent H-bond accepting interactions to 1-AN solvation.

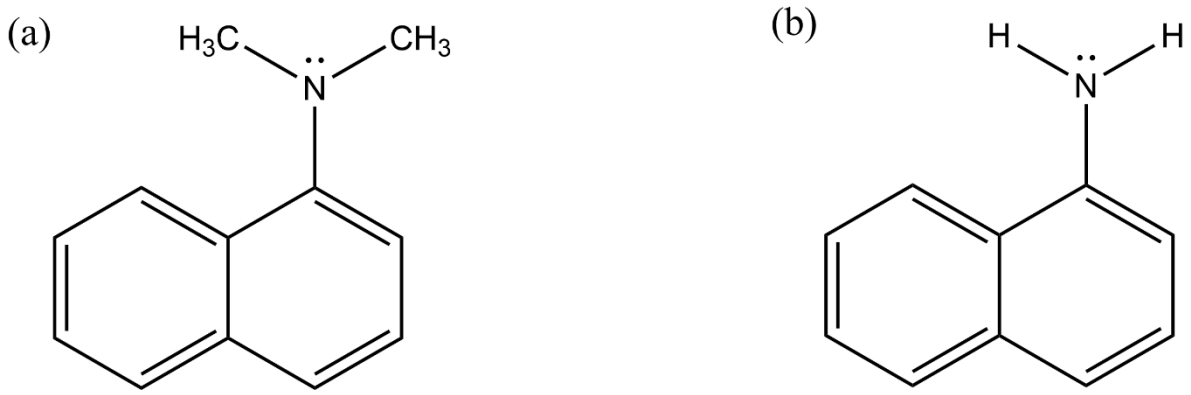

Figure 5. (a) 1-dimethylaminonapthalene (b) aminonapthalene.

The fluorescence of ANs can be schematically represented by the classical Jablonski diagram, which is used to describe the various molecular processes involved in the absorption and emission of light [72-74]. Jablonski diagrams illustrate the electronic states of a fluorophore (e.g. 1-AN) and the transitions occurring between these states. At each energy level, a fluorophore may exist in a number of closely-spaced vibrational energy levels (0,1,2,3,4 etc.) within each electronic state (S_0, S_1, S_2) [72]. Upon photoexcitation, the fluorophore absorbs light and is excited to a higher vibrational energy level, followed by the relaxation of excited electrons back to the ground state (S_0) through internal conversion and photon emission (i.e. fluorescence) [72,73].

Fig. 1 (b) depicts a simplified Jablonski diagram of 1-AN fluorescence in three solvent environments: non-polar, polar, polar and H-bonding. The vertical axis represents increasing energy where 1-AN would typically have an absorbance spectrum. As seen in the illustration, dipole-dipole and H-bonding interactions stabilize the large dipole moment of 1-AN, reducing the overall energy and energy levels within each electronic state. This results in a smaller effective dipole of lower energy.

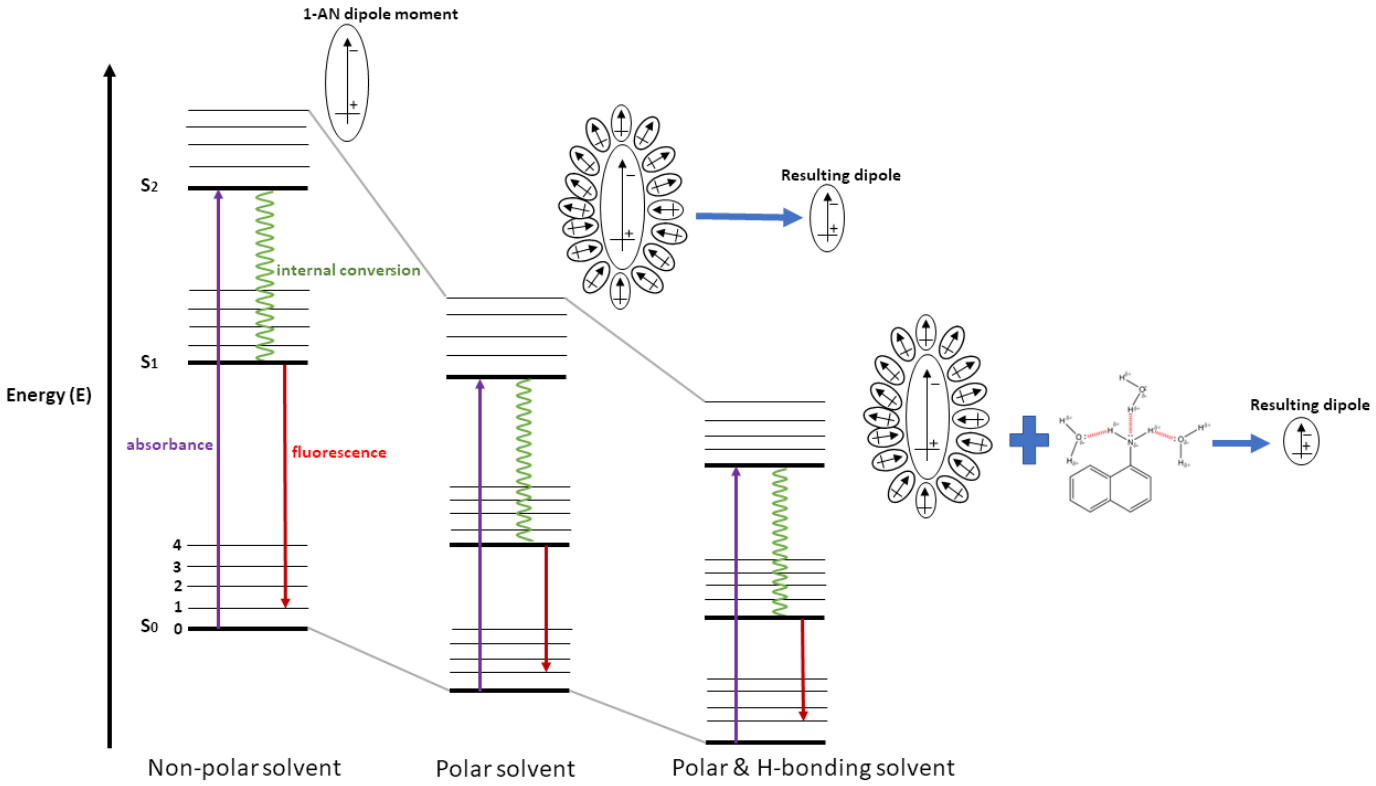

Figure 6. Schematic illustration of 1-aminonapthalene fluorescence in different solvent environments using a Jablonski diagram.

In order to understand how urea affects the solvation of 1-DMAN and 1-AN, we first have to experimentally characterize its solvatochromicity in neat solvents. We have measured the fluorescence spectrum of 1-DMAN and 1-AN in a variety of non-H-bonding and H-bonding solvents (Fig. 7), and have determined their maximum emission wavelength peak position (λ_{max}) by fitting the raw data to a Weibull 5 parameter peak distribution using SigmaPlot data analysis software (Table 2). It is clear from the results that the fluorescence spectrum of these two molecules are solvent dependent.

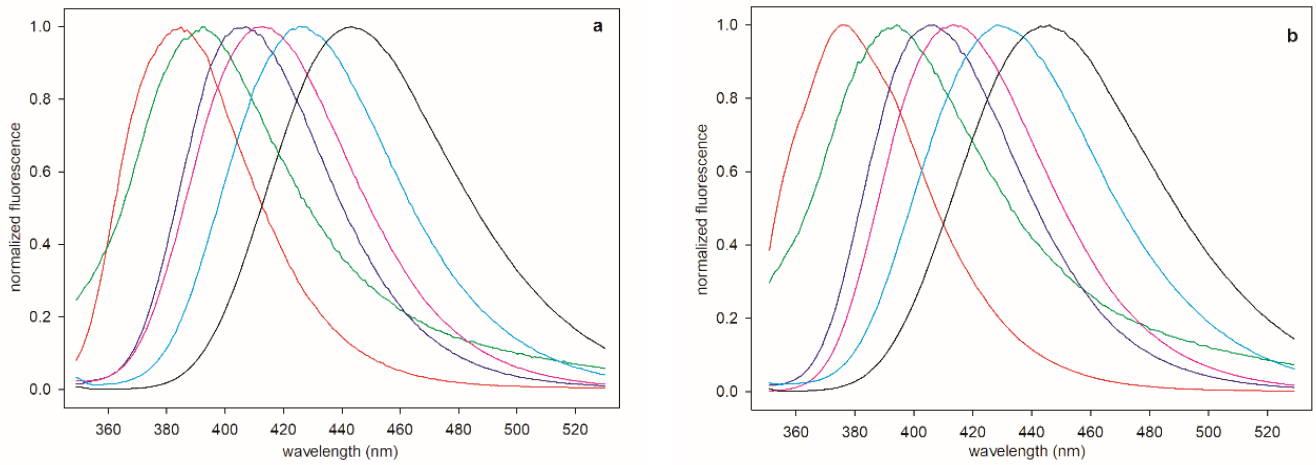

Figure 7. Fluorescence emission spectra (normalized to maximum intensity) of aminonapthalenes in neat solvents of varying polarity and H-bonding abilities. (a) 1-DMAN in hexane, dibutyl ether, ethyl acetate, propanol, ethylene glycol and water (b) 1-AN in hexane, dibutyl ether, ethyl acetate, acetonitrile, ethylene glycol and water, in the order of red, green, blue, purple, cyan, black for both molecules.

3.1.2. Quantification of the Solvatochromism of Aminonapthalenes using the Onsager Solvent Polarity Function

Solvatochromic shifts are related to solvent-solute interactions, and are either caused by non-specific dielectric interactions or result from specific solvent-solute interactions (most often H-bonds) [99]. For 1-DMAN and 1-AN the solvatochromic shifts can be expressed as [85]:

$$\frac{1}{\lambda_{max}} = \frac{1}{\lambda^0_{max}} - \Delta_{dielectric} - \Delta_{H-bond} \qquad (12)$$

λ_{max} is the maximum emission wavelength measured in a given solvent, λ^0_{max} is the maximum emission wavelength measured in vacuum, $\Delta_{dielectric}$ and Δ_{H-bond} are respectively the contributions of solvent-solute dielectric and H-bond interactions to the solvatochromic shift. Dielectric effects upon electronic spectra ($\Delta_{dielectric}$) are well-described by continuum models[85-90] and are shown to be proportional to the Onsager polarity function, which will be used for the quantitative analysis of 1-AN and 1-DMAN solvatochromism.

The Onsager Reaction Field (ORF) model describes the influence between a molecule (e.g. AN) and its surrounding medium (solvent); where induced dipole-dipole interactions generate an opposing reaction field directly proportional to the molecular dipole moment (μ), and inversely proportional to the radius of the solvation shell cavity (a) [91]. The Lippert-Mataga equation uses the theories behind the ORF model to relate fluorescence emission peak energy (J) of a fluorescent molecule in solution to the dielectric constant (ε) of the solvent, where J_0 and ε_0 are the vacuum emission peak energy of the molecule and the vacuum dielectric constant of the solvent respectively. The bracketed term is the Onsager solvent polarity function [90,91].

$$J = -\frac{\Delta\mu^2}{a^3}\cdot\frac{1}{4\pi\,\epsilon_0}\left[\frac{2(\varepsilon-1)}{2\varepsilon+1}\right] + J_0 \qquad (13)$$

As stated earlier, the relationship between emission peak energy and the Onsager solvent polarity function follows a linear correlation [85-91]. However, the ORF model correlation of ANs in H-bonding solvents is expected to deviate from linearity due to energetic contributions from H-bonding interactions, allowing us to quantitatively determine solvent H-bond donor/acceptor properties.

The contribution from H-bond interactions can be partitioned into solvent H-bond donor and solvent H-bond acceptor contributions [92-93]: $\Delta_{H-bond} = \Delta_{donor} + \Delta_{acceptor}$. Eq-12 can therefore be re-written as:

$$\frac{1}{\lambda_{max}} = \frac{1}{\lambda^0_{max}} - \alpha\times\frac{2(\varepsilon-1)}{2\varepsilon+1} - \Delta_{donor} - \Delta_{acceptor} = \frac{1}{\lambda^0_{max}} - a\times\frac{2(\varepsilon-1)}{2\varepsilon+1} - m\alpha - n\beta \qquad (14)$$

Where "*a, m* and *n"* are constants, and Δ_{donor} and $\Delta_{acceptor}$ are assumed to be proportional with the solvent H-bond donor acidity (α) and solvent H-bond acceptor basicity (β)[92,93]. It should be noted that for 1-DMAN that cannot donate H-bonds, $\Delta_{acceptor}$ (and therefore β) is zero.

Fig. 8(a) depicts solvent effects upon the 1-DMAN fluorescence spectrum by plotting $\frac{1}{\lambda_{max}}$ as a function of the Onsager polarity function (Lippert-Mataga plot), using dielectric constants reported in the literature (Table 2) [95]. For non-H-bonding solvents (green points), it can be seen that $\frac{1}{\lambda_{max}}$ correlates linearly with $\frac{2(\varepsilon-1)}{2\varepsilon+1}$, Eq-15 giving the regression line:

$$\left(\frac{1}{\lambda_{max,\ DMAN}}\right)_{dielectric} = (2740000 \pm 20000) + (-350000 \pm 30000) \times \frac{2(\varepsilon-1)}{2\varepsilon+1} \qquad (15)$$

Table 2. 1-AN and 1-DMAN maximum emission wavelengths (λ_{max}) measured in various neat solvents of known dielectric constants with their associated Onsager polarity functions $\frac{2(\varepsilon-1)}{2\varepsilon+1}$.

Solvent	Dielectric constant, (ε)[95]	$\frac{2(\varepsilon-1)}{2\varepsilon+1}$	1-AN λ_{max}	1-DMAN λ_{max}
hexane	1.8800	0.3697	377.21 ± 0.12	383.36 ± 0.07
cyclohexane	2.0200	0.4048	378.03 ± 0.11	383.83 ± 0.07
dibutyl ether	3.1000	0.5833	394.18 ± 0.20	392.53 ± 0.18
diethyl ether	4.2670	0.6853	399.34 ± 0.07	394.63 ± 0.17
chloroheptane	5.5200	0.7508	389.89 ± 0.17	399.43 ± 0.06
chlorohexane	6.1000	0.7727	392.30 ± 0.07	398.00 ± 0.08
ethyl acetate	6.0200	0.7699	406.66 ± 0.08	406.99 ± 0.13
dichloromethane	9.0800	0.8434	400.02 ± 0.09	409.61 ± 0.08
dichloroethane	10.4200	0.8626	401.25 ± 0.09	410.59 ± 0.08
propanol	20.1000	0.9272	425.90 ± 0.05	413.31 ± 0.07
Ethanol	24.6000	0.9402	424.91 ± 0.05	414.87 ± 0.06
Methanol	32.8440	0.9550	426.53 ± 0.04	419.33 ± 0.05
ethylene glycol	37.0000	0.9600	430.12 ± 0.05	426.68 ± 0.06
acetonitrile	36.6017	0.9596	413.98 ± 0.07	420.96 ± 0.06
Water	80.1000	0.9814	445.44 ± 0.09	443.99 ± 0.09

Fig. 8(a) also shows as expected, that the peak energies of 1-DMAN measured in purely H-bond accepting solvents fall within the 95% confidence interval of the regression line defined by Eq-15. However, it can also be seen Fig. 8(a), that as the H-bond donation acidity of the solvent increases [93], the measured $\frac{1}{\lambda_{max}}$ shows a greater deviation from the predicted regression line. This deviation can be used to monitor changes in solvent H-bond donation acidity.

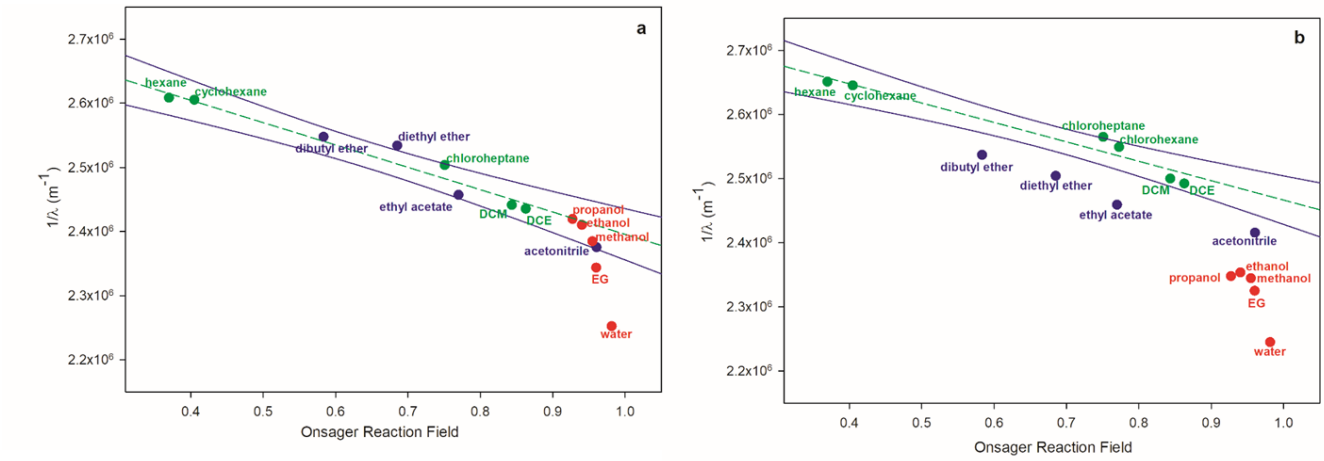

Figure 8. Lippert-Mataga plots of (a) 1-DMAN and (b) 1-AN emission in a variety of non-hydrogen bonding solvents (green circles), purely hydrogen bond acceptor solvents (blue circles), and solvents that both donate and accept hydrogen bonds (red circles) of ranging polarity; abbreviations: DCM (dichloromethane), DCE (dichloroethane) and EG (ethylene glycol). The dashed line represents the best fit to the Lippert-Mataga equation passing through the green data (Eq-15 and Eq-16), solid blue lines represent the 95% confidence interval of the linear regression line.

Fig. 8(b) demonstrates solvent effects upon the fluorescence of 1-AN by plotting $\frac{1}{\lambda_{max}}$ measured in a number of neat solvents as a function of the Onsager polarity function, using dielectric constants from the literature [95]. The peak energies of 1-AN measured in non-H-bonding solvents are well-correlated with the Lippert-Mataga equation giving the regression line:

$$\left(\frac{1}{\lambda_{max,\ AN}}\right)_{dielectric} = (2770000 \pm 20000) + (-300000 \pm 40000) \times \frac{2(\varepsilon-1)}{2\varepsilon+1} \qquad (16)$$

The two correlation lines given by Eq-15 and Eq-16 are essentially identical within error, this is not surprising as both the ground and excited state dipole moments of 1-AN and 1-DMAN are quite close in value [81] to one another. However, as it can be seen in Fig. 8(b), unlike 1-DMAN, the fluorescence spectrum of 1-AN is also sensitive towards solvent H-bond acceptability as well as solvent H-bond donation.

3.1.3. The addition of Urea has a Small Effect on the H-Bond Donation of the Solvent

Given that H-bond donating solvents cause excess redshift in the fluorescence spectrum of 1-DMAN, the constant "*m*" of Eq-14 for this molecule is positive. We have therefore measured the fluorescence spectrum of 1-DMAN in a number of aqueous mixtures, in order to ascertain the effects of co-solvent addition on the H-bond donation properties of aqueous solvent systems. While urea as a co-solvent is the focus of this work, organic solvents like methanol and acetonitrile were used as positive controls to ensure that our system is well-behaved, and our probe is sensitive to relevant parameters. Table 3 (a-d) lists the experimentally determined λ_{max} for 1-DMAN and 1-AN in urea, methanol and acetonitrile-water mixtures and the calculated Onsager polarity functions based on dielectric constants from literature [96-98].

Fig. 9 plots the effects of urea, methanol and acetonitrile addition upon the fluorescence spectrum of 1-DMAN in water. This solvent shift can be represented by:

$$\left(\frac{1}{\lambda_{max,\ DMAN}}\right)_{mixture} - \left(\frac{1}{\lambda_{max,\ DMAN}}\right)_{water} = (-350000 \pm 30000) \times \left(\left(\frac{2(\varepsilon-1)}{2\varepsilon+1}\right)_{mixture} - \left(\frac{2(\varepsilon-1)}{2\varepsilon+1}\right)_{water}\right) - m \times (\alpha_{mixture} - \alpha_{water}) \quad (17)$$

Table 3. 1-AN and 1-DMAN maximum emission wavelengths (λ_{max}) measured in water-co-solvent mixtures of known dielectric constants with their associated Onsager polarity functions, $\frac{2(\varepsilon-1)}{2\varepsilon+1}$.

(a)

Urea [M]	Dielectric constant, (ε)[96]	$\frac{2(\varepsilon-1)}{2\varepsilon+1}$	1-AN λ_{max}	1-DMAN λ_{max}
0.0000	80.1000	0.9814	445.79 ± 0.09	444.67 ± 0.09
0.4711	81.2455	0.9817	445.69 ± 0.09	444.39 ± 0.09
1.0024	82.5373	0.9819	445.65 ± 0.09	444.19 ± 0.09
1.5350	83.8324	0.9822	445.75 ± 0.09	444.12 ± 0.09
1.9503	84.8422	0.9824	445.59 ± 0.09	444.07 ± 0.09
2.4857	86.1440	0.9827	445.24 ± 0.09	443.76 ± 0.09
3.0228	87.4498	0.9829	445.44 ± 0.11	443.81 ± 0.09
4.0120	89.8553	0.9834	445.22 ± 0.09	444.09 ± 0.09
5.0080	92.2768	0.9838	445.00 ± 0.09	443.43 ± 0.08
5.9806	94.6418	0.9842	444.85 ± 0.09	443.33 ± 0.09

(b)

Methanol [M]	Dielectric constant, (ε)[97]	$\frac{2(\varepsilon-1)}{2\varepsilon+1}$	1-AN λ_{max}	1-DMAN λ_{max}
0.0000	80.1000	0.9814	445.44 ± 0.09	443.99 ± 0.09
3.0593	78.6459	0.9810	444.40 ± 0.09	443.18 ± 0.08
6.0218	76.1789	0.9804	442.52 ± 0.08	440.59 ± 0.08
8.8876	72.8063	0.9795	440.00 ± 0.08	437.20 ± 0.08
11.6292	68.6353	0.9783	438.38 ± 0.07	435.78 ± 0.07
14.2306	63.7730	0.9767	436.46 ± 0.07	433.77 ± 0.06
16.6742	58.3266	0.9745	434.33 ± 0.06	430.29 ± 0.06
18.9485	52.4034	0.9716	432.42 ± 0.05	428.35 ± 0.05

(c)

Acetonitrile [M]	Dielectric constant, (ε)[98]	$\frac{2(\varepsilon-1)}{2\varepsilon+1}$	1-AN λ_{max}	1-DMAN λ_{max}
0.0000	80.1000	0.9814	445.44 ± 0.09	443.99 ± 0.09
2.3804	76.7617	0.9806	442.24 ± 0.08	441.69 ± 0.09
4.6693	72.0140	0.9793	436.84 ± 0.06	436.93 ± 0.07
6.8563	67.1765	0.9778	433.18 ± 0.06	432.89 ± 0.07
8.9305	61.9691	0.9760	430.21 ± 0.05	429.76 ± 0.06

Based on experimentally determined dielectric constants (Table 3(a-c)) [95-98], we can estimate the range of values taken on by the Onsager polarity function for our mixtures. For all mixtures in this work, the value of $\frac{2(\varepsilon-1)}{2\varepsilon+1}$ deviates by less than 0.01 relative to that of pure water, allowing us to neglect the first term:

$$\left(\frac{1}{\lambda_{max,\ DMAN}}\right)_{mixture} - \left(\frac{1}{\lambda_{max,\ DMAN}}\right)_{water} \approx -m \times (\alpha_{mixture} - \alpha_{water}) \quad (18)$$

The effect of co-solvent addition upon solvent H-bond acidity can be related to the solvatochromic shift via:

$$\frac{d\left(\frac{1}{\lambda_{max,\ DMAN}}\right)_{mixture}}{d[co-solvent]} = -m\frac{d(\alpha_{mixture})}{d[co-solvent]} \quad (19)$$

The data in Fig. 9 show that in comparison to methanol and acetonitrile, **the addition of urea to water barely affects the solvent H-bond acidity as measured by the 1-DMAN probe** (the slight increase in 1-DMAN emission wavenumber is less than slit width of the measurement). These results are consistent with the results of Gai [69], Dougan[100] and Cremer [45], demonstrating that urea addition has an almost negligible effect on the H-bond donation properties of the solvent. Therefore, urea cannot denature proteins through H-bond donation interactions with the protein backbone.

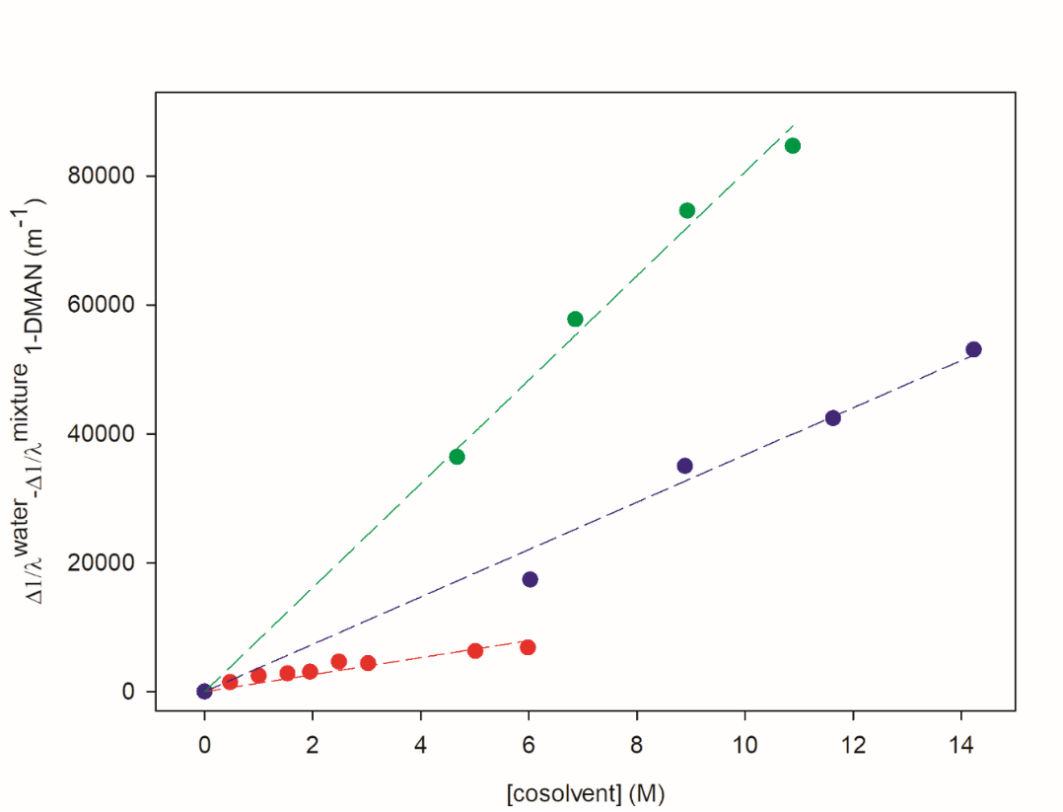

Figure 9. Solvent emission peak shifts of 1-DMAN observed relative to pure water, measured in binary aqueous mixtures of urea (red circles), methanol (blue circles), and acetonitrile (green circles). The lines represent the best linear fits to each set of data.

3.1.4. Urea has No Significant Influence on the Acceptance of H-Bonds in Solvents

The sensitivity of 1-AN to both solvent H-bond acceptance and donation can be used to quantify how co-solvent addition to water changes its H-bond acceptability. Using arguments similar to those used for deriving Eq-18:

$$\left(\frac{1}{\lambda_{max,\ AN}}\right)_{mixture} - \left(\frac{1}{\lambda_{max,\ AN}}\right)_{water} \approx -m' \times (\alpha_{mixture} - \alpha_{water}) - n' \times (\beta_{mixture} - \beta_{water}) \quad (20)$$

Where m' and n' are constants; substituting Eq-18 in Eq-20:

$$\left(\frac{1}{\lambda_{max,\ AN}}\right)_{mixture} - \left(\frac{1}{\lambda_{max,\ AN}}\right)_{water} \approx \frac{m\prime}{m} \times \left(\left(\frac{1}{\lambda_{max,\ DMAN}}\right)_{mixture} - \left(\frac{1}{\lambda_{max,\ DMAN}}\right)_{water}\right) - n' \times (\beta_{mixture} - \beta_{water}) \quad (21)$$

Calculations[94] as well as experimental results[92], show that although the nitrogen atom of primary amine groups functions as a good H-bond acceptor for the hydrogen atoms of water, the amine hydrogens are poor H-bond donors for oxygens atoms of water. Therefore, at low concentrations of co-solvent, the second term in Eq-21 can be ignored and $\left(\frac{1}{\lambda_{max,\ AN}}\right)_{mixture} - \left(\frac{1}{\lambda_{max,\ AN}}\right)_{water}$ will linearly depend upon $\left(\frac{1}{\lambda_{max,\ DMAN}}\right)_{mixture} - \left(\frac{1}{\lambda_{max,\ DMAN}}\right)_{water}$. However, as concentration of co-solvent increases, induced perturbations in solvent H-bond acceptability should cause appreciable deviation from linearity.

We have plotted $\left(\frac{1}{\lambda_{max,\ AN}}\right)_{mixture} - \left(\frac{1}{\lambda_{max,\ AN}}\right)_{water}$ as a function of $\left(\frac{1}{\lambda_{max,\ DMAN}}\right)_{mixture} - \left(\frac{1}{\lambda_{max,\ DMAN}}\right)_{water}$ for urea-water, methanol-water and acetonitrile-water mixtures, as depicted in Fig. 10. It can be clearly seen that unlike other co-solvents, urea addition minimally perturbs the fluorescence peak energy of 1-AN, and exhibits no appreciable deviation from linear behavior compared to data uncertainty. **Therefore, as far as the 1-AN probe is concerned, the addition of urea does not affect the H-bond acceptance of the aqueous solvent.**

In contrast, in methanol-water and acetonitrile-water mixtures, the dependence of $\left(\frac{1}{\lambda_{max,\ AN}}\right)_{mixture} - \left(\frac{1}{\lambda_{max,\ AN}}\right)_{water}$ upon $\left(\frac{1}{\lambda_{max,\ DMAN}}\right)_{mixture} - \left(\frac{1}{\lambda_{max,\ DMAN}}\right)_{water}$ negatively deviates from linearity at concentrations above 4 M acetonitrile. Unlike urea, acetonitrile causes an increase in solvent H-bond acceptability that is clearly detectable by the 1-AN probe. However, it is also clear from Fig. 10 that it is the change in solvent H-bond donation that dominates co-solvent effects upon the solvation of 1-AN.

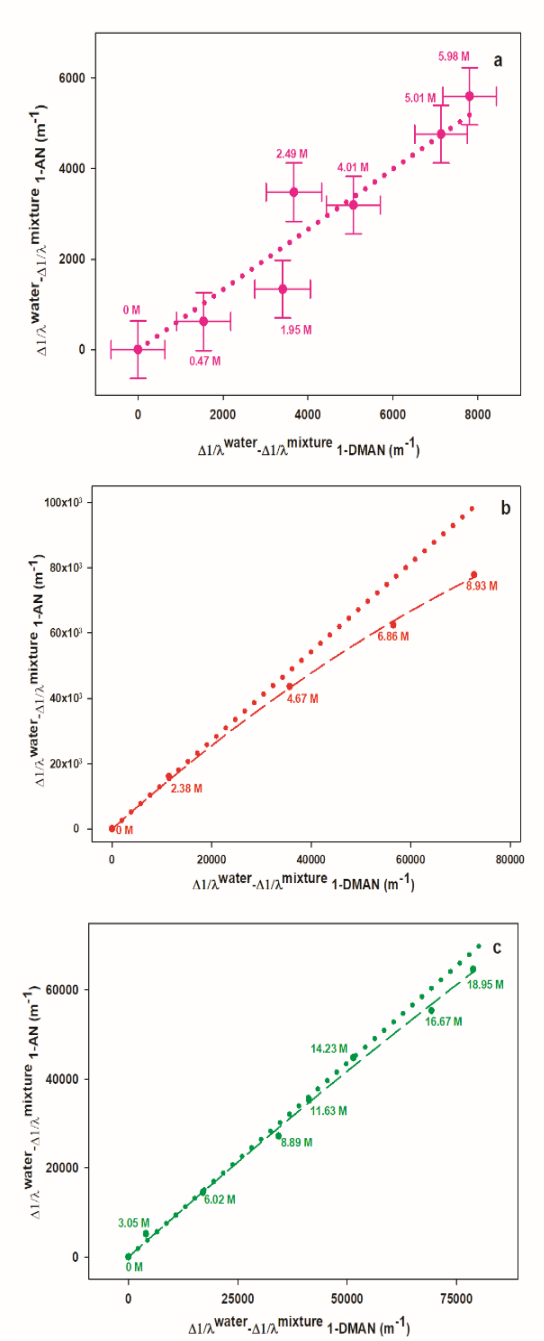

Figure 10. Solvent emission peak shifts (relative to pure water) of 1-AN measured in binary aqueous mixtures, plotted against commensurate values of 1-DMAN; a) urea-water, b) acetonitrile-water, and c) methanol-water mixtures.

References

81. Lewis, F. D. Formation and anomalous behavior of Aminonaphthalene− Cinnamonitrile exciplexes. *The Journal of Physical Chemistry.* (2000); 104 (15), 3261–3268.
82. Rückert, I., Demeter, A., Morawski, O., Kühnle, W., Tauer, E., Zachariasse, K. A. Internal Conversion in 1-Aminonaphthalenes. Influence of Amino Twist Angle. *The Journal of Physical Chemistry A.* (1999); *103* (13), 1958-1966.
83. Rosenberg, H. M. Eimutis, E, Solvent shifts in electronic spectra—I. Stokes shift in a series of homologous aromatic amines. *Spectrochimica Acta.* (1966); *22* (10), 1751-1757.
84. Hong, C., Yun-Bao, J. Photophysics of 1-dimethylaminonaphthalene in aqueous-organic binary solvents. *Chemical Physics Letters* **(**2000); *325* (5-6) , 605-609.
85. Khajehpour, M., Welch, C. M., Kleiner, K. A., Kauffman, J. F. Separation of Dielectric Nonideality from Preferential Solvation in Binary Solvent Systems: An Experimental Examination of the Relationship between Solvatochromism and Local Solvent Composition around a Dipolar Solute. *The Journal of Physical Chemistry A.* (2001); *105* (22), 5372-5379.
86. Lippert, E. Spectroscopic determination of the dipole moment of aromatic compounds in the first excited singlet state. *Z. Elektrochem* (1957); *61* (8), 962-975.
87. Mataga, N., Kaifu, Y., Koizumi, M. Solvent Effects upon Fluorescence Spectra and the Dipolemoments of Excited Molecules. *Bulletin of the Chemical Society of Japan* (1956); *29* (4), 465-470.
88. Suppan, P., Tsiamis, C. Absolute excited state dipole moments from solvatochromic shifts. *Spectrochimica Acta Part A: Molecular Spectroscopy.* (1980); *36* (11), 971-974.
89. Suppan, P. Excited-state dipole moments from absorption/fluorescence solvatochromic ratios. *Chemical Physics Letters.* (1983); *94* (3), 272-275.

90. Khajehpour, M., Kauffman, J.F. Dielectric enrichment of 1-(9-Anthryl)-3-(4-N,N-dimethylaniline) propane in hexane−ethanol mixtures. *The Journal of Physical Chemistry A* **(**2000)**;** *104*(30), 7151-7159.

91. Thomas, H., Brout, R. Molecular field theory, the Onsager reaction field, and the spherical model. *Journal of Applied Physics*. (1968); 39 (2), 624–625.

92. Kamlet, M. J., Taft, R. W. The solvatochromic comparison method. I. The .beta.-scale of solvent hydrogen-bond acceptor (HBA) basicities. *Journal of the American Chemical Society.* (1976); *98* (2), 377-383.

93. Taft, R. W., Kamlet, M. J. The solvatochromic comparison method. 2. The .alpha.-scale of solvent hydrogen-bond donor (HBD) acidities. *Journal of the American Chemical Society.* (1976); *98* (10), 2886-2894.

94. Hoehn, R. D., Carignano, M. A., Kais, S., Zhu, C., Zhong, J., Zeng, X. C., Francisco, J. S., Gladich, I. Hydrogen bonding and orientation effects on the accommodation of methylamine at the air-water interface. *The Journal of Chemical Physics* (2016), *144*, 214701.

95. CRC handbook of chemistry and physics. Chapman and Hall/CRCnetBASE: Boca Raton, FL, 1999; pp CD-ROMs.

96. Wyman, J., Dielectric Constants: Ethanol—Diethyl Ether and Urea—Water Solutions between 0 and 50°. *Journal of the American Chemical Society.* (1933); *55* (10), 4116-4121.

97. Agmon, N., Huppert, D., Masad, A., Pines, E. Excited-state proton transfer to methanol-water mixtures. *The Journal of Physical Chemistry.* (1991); *95* (25), 10407-10413.

98. Gagliardi, L. G., Castells, C. B., Ràfols, C., Rosés, M., Bosch, E. Static Dielectric Constants of Acetonitrile/Water Mixtures at Different Temperatures and Debye−Hückel A and a0B

Parameters for Activity Coefficients. *Journal of Chemical & Engineering Data.* (2007); *52* (3), 1103-1107.

99. Suppan, P. Invited review solvatochromic shifts: The influence of the medium on the energy of electronic states. *Journal of Photochemistry and Photobiology A: Chemistry.* (1990); *50* (3), 293-330.

100. Nasralla, M.; Laurent, H.; Baker, D.; Ries, M. E.; Dougan, L., A study of the interaction between TMAO and urea in water using NMR spectroscopy. *Physical Chemistry Chemical Physics*. (2002).

Part II: Determination of the Effects of Urea Addition on Intramolecular H-bonding

3.2.1. Measuring The Intramolecular H-Bond Strength of *ortho*-hydroxybenzoic acid

Next, we study the putative disruptive effect of urea upon intra-molecular H-bonding by measuring how adding urea perturbs the dissociation constants (K_a) of *ortho*- and *para*-hydroxybenzoic acid (Fig. 11). *o*-HBA can form a strong intramolecular H-bond between the *ortho* hydroxyl and carboxylate substituents in the closing of its six-member ring (Fig. 11(c), Scheme I), while *p*-HBA cannot form the intramolecular H-bond [101,102]. As a result, *p*-HBA is stabilized by dipole-dipole and intermolecular H-bonding interactions, and *o*-HBA is additionally stabilized by intramolecular H-bonding interactions. Both ionization states of *o*-HBA form the intramolecular H-bond, but the charged H-bonds behave slightly differently from the uncharged H-bonds depending on solvent properties [101-103].

With changes in solvent polarity and H-bond abilities, any change in the $K_{a(int)}$ of *o*-HBA is proportional to changes in the $K_{a(int)}$ of *p*-HBA. However, the change in $K_{a(obs)}$ of *o*-HBA accounts additionally for intramolecular H-bonding interactions [102]. The strength of the *o*-HBA intramolecular H-bond can be represented by the equilibrium constant K_H whose magnitude can be related to pK_a values of *o*-HBA and *p*-HBA through [102]:

$$\log K_H = pK_{(p-\mathrm{HBA})} - pK_{(o-\mathrm{HBA})} \qquad (22)$$

Any shift in K_H with change in solvent properties represents a change in intramolecular H-bond strength [102]. The pK_a values of the COOH groups in *o*-HBA and *p*-HBA can be accurately determined by measuring the change in UV absorbance as ionization occurs, known as spectrophotometric titration [102]. In this study, we measure the effect of urea on the intramolecular H-bond strength of *o*-HBA in water.

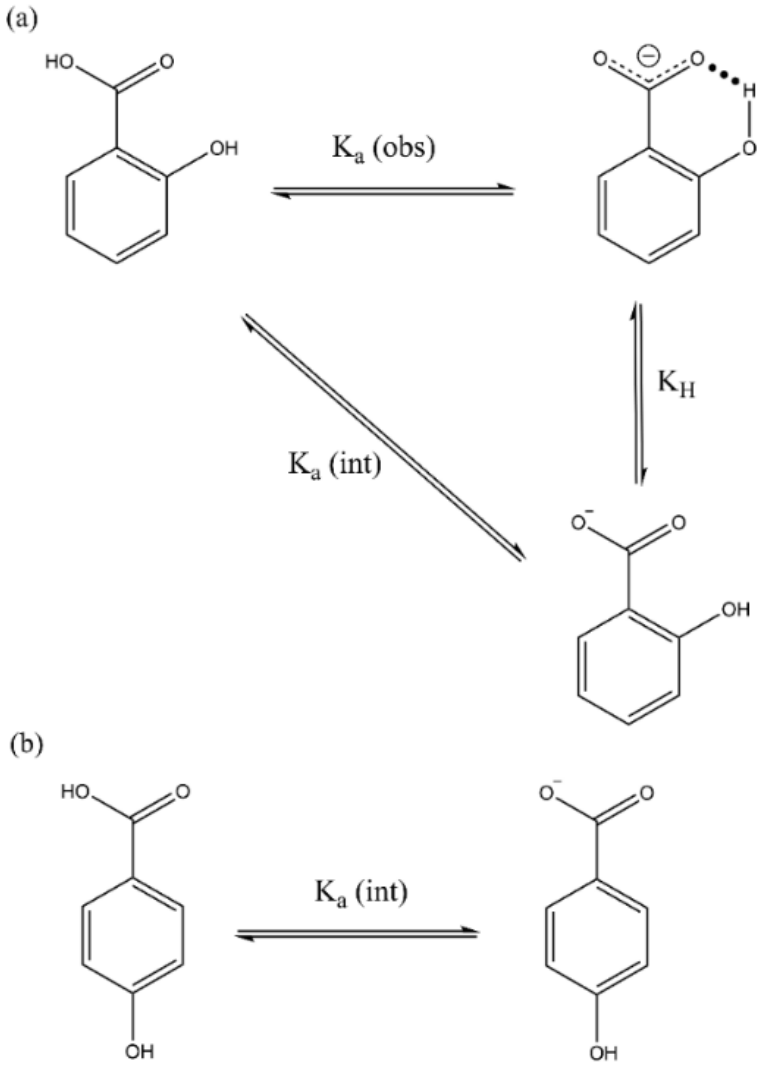

Figure 11. Scheme (I). Thermodynamic cycle (a) representing the effect of intramolecular hydrogen bonding on the overall dissociation constant of *o*-HBA, K_a(obs). In this scheme, the value of K_a(int) is assumed to be close to the dissociation constant of *p*-HBA (b). The equilibrium constant K_H can be used to represent the strength of intramolecular hydrogen bonding between the carboxylate and hydroxyl moieties in *o*-HBA.

3.2.2. pH Determination with Fluorine NMR Spectroscopy

Nominally, the K_a of a monoprotic acid (*HA*) relates to the pH via:

$$log\frac{[A^-]}{[HA]} = logK_a + log\frac{\gamma_{HA}}{\gamma_{A^-}} - \log(a_H) \qquad (23)$$

Where K_a is the dissociation constant of the acid measured in pure water, a_H is the activity of the hydronium ion, while γ_{HA} and γ_{A^-} are the activity coefficients of the acidic and basic forms of *HA*. Equation 23 is of limited use in mixed solvent systems because of the challenges associated with directly measuring pH at high concentrations of organic co-solvent [104-105]. To circumvent this problem for *o*-HBA and *p*-HBA, we have the method of Frohlinger [106] by adding a small amount of fluoride ion to our buffer system that functions as an NMR pH probe [78]. Equation 23 can then be re-written as:

$$log\frac{[A^-]}{[HA]} = logK_a + log\frac{\gamma_{HA}}{\gamma_{A^-}} - \log K_{HF} - \log\frac{\gamma_{HF}}{\gamma_{F^-}} + \log\frac{[F^-]}{[HF]} = \ (\mathrm{p}K_{HF}^{apparent} - \mathrm{p}K_{HA}^{apparent}) + \log\frac{[F^-]}{[HF]} \qquad (24)$$

Where $\frac{[F^-]}{[HF]} = (\frac{\delta_{F-} - \delta_{obs}}{\delta_{obs} - \delta_{HF}})$, K_{HF} is the dissociation constant of HF in pure water, γ_{HF} is the activity coefficient of HF, γ_{F^-} is the activity coefficient of fluoride ion, δ_{F-} and δ_{HF} are the F-NMR chemical shifts of pure fluoride and pure hydrogen fluoride and δ_{obs} is the F-NMR chemical shift measured for a solution of interest. Figure 12 depicts the titration of fluoride ion measured at various pHs.

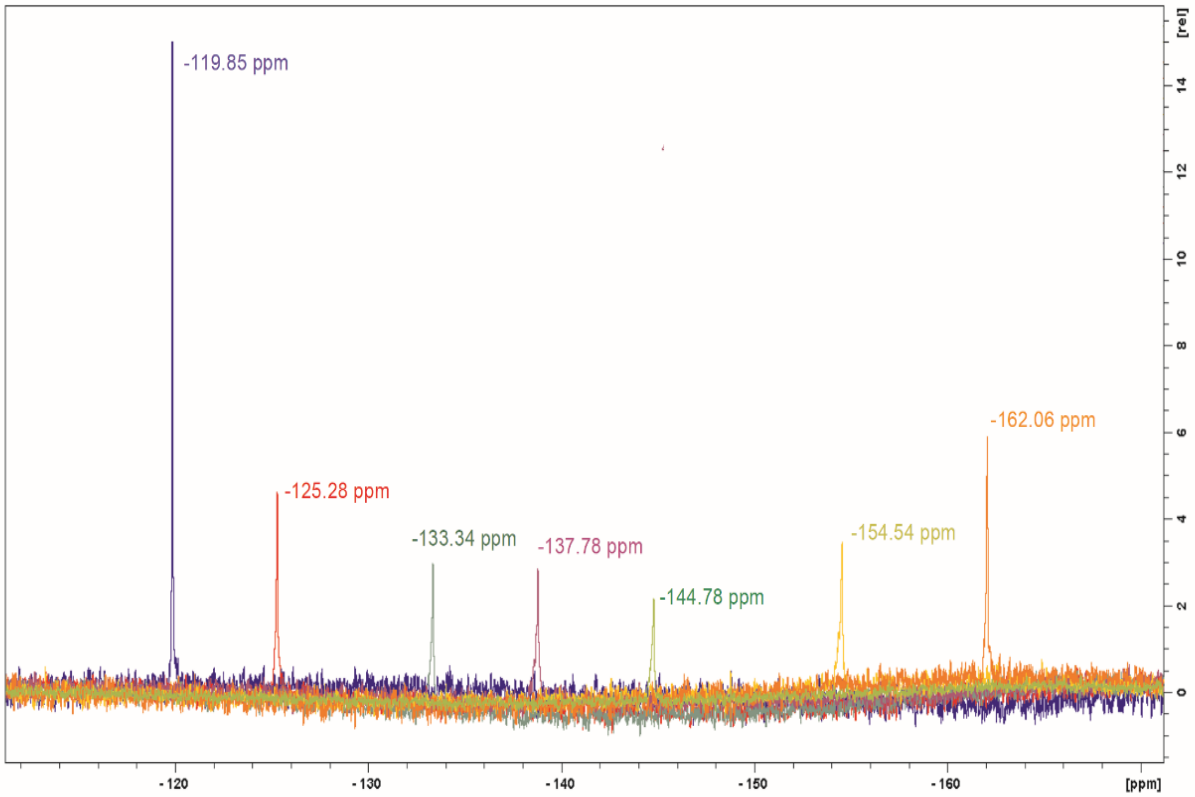

Figure 12. Fluorine NMR spectra depicting the chemical shifts (δ) of fluoride ion (2 mM potassium fluoride in 50 mM sodium formate). Peaks from right to left: pH 1.00, 2.50, 3.00, 3.25, 3.50, 4.00, 7.00.

3.2.3. Isosbestic Point Determination of *o*-HBA and *p*-HBA

UV-absorbance spectra of *o*-HBA and *p*-HBA were measured at different pH values to determine the isosbestic point (i.e., the wavelength where the uncharged and charged species in an $HA \rightleftharpoons A^-$ equilibrium have the same absorption) [75]. This allows us to allows us to correct for variations in probe concentration. Figure 13 depicts the spectrophotometric titration of *o*-HBA and *p*-HBA in water. *o*-HBA is observed to have 3 isosbestic points in its absorbance spectra. The isosbestic point at 300nm was chosen for normalization, as background interferences from co-solvents (e.g. urea, methanol) and impurities are usually higher below 250 nm. Only one isosbestic point was observed for *p*-HBA at 247 nm.

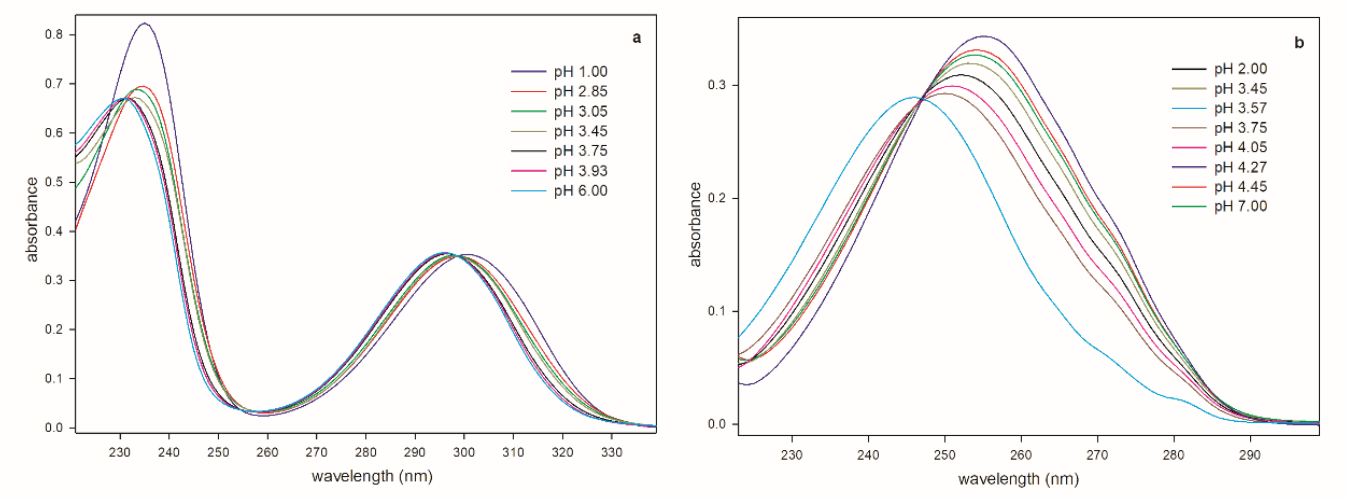

Figure 13. The pH dependence of absorbance spectra of: (a) 100 uM *o*-HBA and (b) 25 uM *p*-HBA in measured in the presence of 2 mM (F^-plus HF), 50 mM (formate plus formic acid).

3.2.4. Urea Does Not Affect The Intramolecular H-bonding Strength of *o*-HBA

We have measured the effect of urea and methanol addition upon the pH dependence of the absorbance spectra of *o*-HBA and *p*-HBA. Methanol was chosen as the control co-solvent because at concentrations below 14 M it only affects the solvent H-bond donation. The UV difference spectra of *o*-HBA and *p*-HBA titration in co-solvent-water mixtures were measured at 310 and 261 nm respectively, and the absorbances were normalized by dividing by the isosbestic point absorbances at 300 and 247 nm. Equation 25 relates the difference in normalized absorbance to the $\frac{[F^-]}{[HF]}$ ratio:

$$Log\left(\frac{A_{obs}-A_{acid}}{A_{basic-}-A_{acid}}\right) = log\frac{[A^-]}{[HA]} = \left(\mathrm{p}K_{HF}^{apparent} - \mathrm{p}K_{HA}^{apparent}\right) + Log\left(\frac{[F^-]}{[HF]}\right) \quad (25)$$

A_{obs} the normalized absorbance of a given sample measured at 310 nm for *o*-HBA and 261 nm for *p*-HBA, A_{acid} the normalized absorbance of the acidic form (at pH 1) measured at 310 nm for o-HBA and 261 nm for *p*-HBA, and A_{basic} the normalized absorbance of the basic form (at pH 7)

measured at 310 nm for *o*-HBA and 261 nm for *p*-HBA. Tables 4 and 5 list the $\frac{[F^-]}{[HF]}$ ratios and absorbances measured for all *o*-HBA and *p*-HBA titrations in urea-water mixtures and methanol-water mixtures respectively.

Table 4 (a-d). Fluorine NMR chemical shifts and UV-absorbance spectra of *o*-HBA and *p*-HBA titrations measured in urea-water mixtures.

(a) 0.00M Urea						
Apparent pH (electrode)	chemical shift (δ) (ppm)	$\frac{[F^-]}{[HF]}$	*o*-HBA Isosbestic point absorbance @ 300 nm	*o*-HBA absorbance @ 310 nm	Normalized absorbance ($\frac{A_{310}}{A_{300}}$)	$(\frac{A_{obs}-A_{acid}}{A_{basic-}-A_{acid}}) = \frac{[A^-]}{[HA]}$
1.00	-162.0540	0.0	0.5571	0.4966	0.8914	0.0
1.50	-161.3160	0.0178	0.5650	0.4990	0.8832	0.0258
2.00	-159.2180	0.0720	0.5585	0.4808	0.8610	0.1030
2.25	-157.2950	0.1271	0.5493	0.4619	0.8409	0.1836
2.50	-154.5100	0.2176	0.5463	0.4455	0.8156	0.3032
2.75	-150.8000	0.3636	0.5540	0.4326	0.7809	0.5135
3.00	-144.7600	0.6942	0.5488	0.4002	0.7291	0.9924
3.25	-138.8900	1.2165	0.5375	0.3676	0.6839	1.7533
3.50	-133.3300	2.1305	0.5340	0.3443	0.6448	3.1143
4.00	-125.3200	6.7131	0.5324	0.3168	0.5949	10.0946
4.50	-121.7690	20.9708	0.5312	0.3054	0.5750	33.3331
7.00	-119.8480	N/A	0.5338	0.3019	0.5656	N/A
Apparent pH (electrode)	chemical shift (δ) (ppm)	$\frac{[F^-]}{[HF]}$	*p*-HBA Isosbestic point absorbance @ 247 nm	*p*-HBA absorbance @ 261 nm	Normalized absorbance ($\frac{A_{310}}{A_{300}}$)	$(\frac{A_{obs}-A_{acid}}{A_{basic-}-A_{acid}}) = \frac{[A^-]}{[HA]}$
1.00	-162.0540	0.0	0.3390	0.3651	1.0770	0.0
2.50	-154.5100	0.2176	0.3292	0.3532	1.0730	6.6774e-3
3.00	-144.7600	0.6942	0.3242	0.3437	1.0603	0.0284
3.25	-138.8900	1.2165	0.3330	0.3486	1.0469	0.0526
3.50	-133.3300	2.1305	0.3389	0.3475	1.0254	0.0938
3.75	-128.6220	3.8103	0.3392	0.3357	0.9897	0.1698
4.00	-125.3200	6.7131	0.3293	0.3079	0.9352	0.3085
4.25	-123.2630	11.3590	0.3352	0.2923	0.8721	0.5170
4.50	-121.7690	20.9708	0.3338	0.2601	0.7793	0.9809
4.75	-120.9460	37.4390	0.3321	0.2308	0.6948	1.7449
5.00	-120.4670	67.1842	0.3335	0.2075	0.6223	3.1028
7.00	-119.8480	N/A	0.3423	0.1628	0.4758	N/A

(b) 2.07 M Urea

Apparent pH (electrode)	chemical shift (δ) (ppm)	$\frac{[F^-]}{[HF]}$	*o*-HBA Isosbestic point absorbance @ 300 nm	*o*-HBA absorbance @ 310 nm	Normalized absorbance ($\frac{A_{310}}{A_{300}}$)	$(\frac{A_{obs}-A_{acid}}{A_{basic-}-A_{acid}}) = \frac{[A^-]}{[HA]}$
1.00	-161.2300	0.0	0.4694	0.4271	0.9099	0.0
1.50	-160.0900	0.0276	0.4715	0.4247	0.9007	0.0290
2.00	-158.4990	0.0689	0.4738	0.4184	0.8832	0.0887
2.25	-156.7990	0.1167	0.4655	0.4015	0.8625	0.1687
2.50	-153.5000	0.2230	0.4664	0.3871	0.8301	0.3213
2.75	-149.9900	0.3608	0.4606	0.3653	0.7930	0.5530
3.00	-144.9360	0.6243	0.4583	0.3422	0.7467	0.9891
3.25	-138.6840	1.1360	0.4540	0.3165	0.6971	1.8439
3.50	-132.4370	2.1173	0.4585	0.2999	0.6540	3.5356
4.00	-124.2770	6.7941	0.4661	0.2824	0.6060	12.4984
4.50	-121.0870	17.8493	0.4563	0.2689	0.5893	41.5859
7.00	-118.8380	N/A	0.4651	0.2705	0.5816	N/A
Apparent pH (electrode)	chemical shift (δ) (ppm)	$\frac{[F^-]}{[HF]}$	*p*-HBA Isosbestic point absorbance @ 247 nm	*p*-HBA absorbance @ 261 nm	Normalized absorbance ($\frac{A_{310}}{A_{300}}$)	$(\frac{A_{obs}-A_{acid}}{A_{basic-}-A_{acid}}) = \frac{[A^-]}{[HA]}$
1.00	-161.2300	0.0	0.2929	0.3326	1.1357	0.0
2.50	-153.5000	0.2230	0.2930	0.3300	1.1264	0.0147
3.00	-144.9360	0.6243	0.3009	0.3346	1.1122	0.0379
3.25	-138.6840	1.1360	0.2862	0.3148	1.0999	0.0587
3.50	-132.4370	2.1173	0.2896	0.3113	1.0751	0.1037
3.75	-127.7100	3.7782	0.2876	0.2802	0.9741	0.3341
4.00	-124.2770	6.7941	0.2942	0.2453	0.8339	0.8788
4.25	-122.2400	11.4609	0.2808	0.2902	1.0338	0.1876
4.50	-121.0870	17.8493	0.2945	0.2662	0.9037	0.5615
4.75	-120.0290	34.5936	0.3026	0.2252	0.7441	1.5440
5.00	-119.5200	61.1584	0.2959	0.1952	0.6598	2.8102
7.00	-118.8380	N/A	0.2997	0.1470	0.4904	N/A

(c) 3.98 M Urea

Apparent pH (electrode)	chemical shift (δ) (ppm)	$\frac{[F^-]}{[HF]}$	*o*-HBA Isosbestic point absorbance @ 300 nm	*o*-HBA absorbance @ 310 nm	Normalized absorbance ($\frac{A_{310}}{A_{300}}$)	$(\frac{A_{obs}-A_{acid}}{A_{basic-}-A_{acid}}) = \frac{[A^-]}{[HA]}$
1.00	-159.5790	0.0	0.4145	0.3832	0.9245	0.0
1.50	-159.1980	9.2160e-3	0.4189	0.3849	0.9190	0.0167
2.00	-157.9100	0.0417	0.4011	0.3597	0.8969	0.0895
2.25	-156.9440	0.0674	0.4168	0.3704	0.8889	0.1185
2.50	-155.2850	0.1147	0.4032	0.3482	0.8637	0.2205
2.75	-152.1240	0.2176	0.3986	0.3299	0.8277	0.4036
3.00	-149.4920	0.3189	0.4118	0.3306	0.8027	0.5666
3.25	-143.2430	0.6435	0.4080	0.3027	0.7419	1.1854
3.50	-137.8250	1.0894	0.4088	0.2873	0.7027	1.9306
4.00	-127.4180	3.3638	0.3898	0.2459	0.6308	6.8189
4.50	-121.3650	10.8934	0.4069	0.2459	0.6043	19.3544
7.00	-117.8570	N/A	0.4008	0.2356	0.5877	N/A
Apparent pH (electrode)	chemical shift (δ) (ppm)	$\frac{[F^-]}{[HF]}$	*p*-HBA Isosbestic point absorbance @ 247 nm	*p*-HBA absorbance @ 261 nm	Normalized absorbance ($\frac{A_{310}}{A_{300}}$)	$(\frac{A_{obs}-A_{acid}}{A_{basic-}-A_{acid}}) = \frac{[A^-]}{[HA]}$
1.00	-159.5790	0.0	0.2807	0.3299	1.1752	0.0
2.50	-155.2850	0.1147	0.2804	0.3278	1.1690	9.3176e-3
3.00	-149.4920	0.3189	0.2876	0.3336	1.1600	0.0231
3.25	-143.2430	0.6435	0.2880	0.3293	1.1431	0.0502
3.50	-137.8250	1.0894	0.2903	0.3273	1.1272	0.0769
3.75	-131.9170	1.9674	0.2937	0.3247	1.1054	0.1160
4.00	-127.4180	3.3638	0.2779	0.2994	1.0773	0.1707
4.25	-123.6410	6.2133	0.2900	0.2923	1.0079	0.3317
4.50	-121.3650	10.8934	0.3028	0.2814	0.9296	0.5765
4.75	-119.9360	19.0683	0.2947	0.2467	0.8372	1.0129
5.00	-119.0640	33.5667	0.3009	0.2235	0.7429	1.8056
7.00	-117.8570	N/A	0.2847	0.1433	0.5035	N/A

(d) 5.98 M Urea						
Apparent pH (electrode)	chemical shift (δ) (ppm)	$\frac{[F^-]}{[HF]}$	*o*-HBA Isosbestic point absorbance @ 300 nm	*o*-HBA absorbance @ 310 nm	Normalized absorbance ($\frac{A_{310}}{A_{300}}$)	$(\frac{A_{obs}-A_{acid}}{A_{basic-}-A_{acid}}) = \frac{[A^-]}{[HA]}$
1.00	-158.7290	0.0	0.3412	0.3200	0.9380	0.0
1.50	-158.1050	0.0150	0.3394	0.3163	0.9320	0.0176
2.00	-157.1200	0.0397	0.3383	0.3097	0.9153	0.0708
2.25	-156.5610	0.0542	0.3532	0.3214	0.9099	0.0891
2.50	-155.3400	0.0874	0.3361	0.2987	0.8889	0.1673
2.75	-153.4550	0.1430	0.3372	0.2908	0.8625	0.2827
3.00	-150.8300	0.2306	0.3343	0.2772	0.8292	0.4654
3.25	-146.4800	0.4095	0.3357	0.2626	0.7823	0.8329
3.50	-140.5200	0.7603	0.3376	0.2460	0.7286	1.5715
4.00	-129.8210	2.1816	0.3255	0.2118	0.6506	5.2027
4.50	-120.7400	9.1101	0.3312	0.2006	0.6058	31.7483
7.00	-116.5700	N/A	0.3318	0.1975	0.5953	N/A
Apparent pH (electrode)	chemical shift (δ) (ppm)	$\frac{[F^-]}{[HF]}$	*p*-HBA Isosbestic point absorbance @ 247 nm	*p*-HBA absorbance @ 261 nm	Normalized absorbance ($\frac{A_{310}}{A_{300}}$)	$(\frac{A_{obs}-A_{acid}}{A_{basic-}-A_{acid}}) = \frac{[A^-]}{[HA]}$
1.00	-158.7290	0.0	0.2940	0.3576	1.2162	0.0
2.50	-155.3400	0.0874	0.2951	0.3563	1.2073	0.0127
3.00	-150.8300	0.2306	0.2969	0.3547	1.1948	0.0314
3.25	-146.4800	0.4095	0.2925	0.3494	1.1943	0.0321
3.50	-140.5200	0.7603	0.2913	0.3439	1.1804	0.0537
3.75	-135.3200	1.2485	0.2880	0.3355	1.1650	0.0786
4.00	-129.8210	2.1816	0.2960	0.3359	1.1348	0.1311
4.25	-124.8700	4.0794	0.3059	0.3299	1.0786	0.2439
4.50	-120.7400	9.1101	0.3030	0.2937	0.9695	0.5421
4.75	-118.1000	26.5549	0.3089	0.2539	0.8218	1.2825
5.00	-117.5800	40.7416	0.3064	0.2278	0.7437	2.0602
7.00	-116.5700	N/A	0.3168	0.1630	0.5144	N/A

Table 5 (a-e). Fluorine NMR chemical shifts and UV-absorbance spectra of *o*-HBA and *p*-HBA titrations measured in methanol-water mixtures.

(a) 0.00M Methanol						
Apparent pH (electrode)	chemical shift (δ) (ppm)	$\frac{[F^-]}{[HF]}$	*o*-HBA Isosbestic point absorbance @ 300 nm	*o*-HBA absorbance @ 310 nm	Normalized absorbance ($\frac{A_{310}}{A_{300}}$)	$(\frac{A_{obs}-A_{acid}}{A_{basic-}-A_{acid}}) = \frac{[A^-]}{[HA]}$
1.00	-161.6990	0.0	0.3103	0.2758	0.8889	0.0
1.50	-160.7400	0.0234	0.3051	0.2683	0.8796	0.0298
2.00	-159.1700	0.0931	0.3129	0.2669	0.8531	0.1247
2.25	-155.5640	0.1714	0.3089	0.2554	0.8267	0.2389
2.50	-154.5700	0.2008	0.3086	0.2446	0.7927	0.4248
2.75	-147.6070	0.5062	0.3076	0.2314	0.7524	0.7328
3.00	-145.7100	0.6000	0.3057	0.2160	0.7067	1.2961
3.25	-139.0500	1.1330	0.2993	0.1994	0.6661	2.2302
3.50	-133.9300	1.8675	0.3000	0.1905	0.6350	3.6930
4.00	-125.3300	5.8005	0.2983	0.1757	0.5891	13.0728
4.50	-120.8830	22.3895	0.3017	0.1740	0.5767	29.8152
7.00	-119.0600	N/A	0.2914	0.1650	0.5662	N/A
Apparent pH (electrode)	chemical shift (δ) (ppm)	$\frac{[F^-]}{[HF]}$	*p*-HBA Isosbestic point absorbance @ 247 nm	*p*-HBA absorbance @ 261 nm	Normalized absorbance ($\frac{A_{310}}{A_{300}}$)	$(\frac{A_{obs}-A_{acid}}{A_{basic-}-A_{acid}}) = \frac{[A^-]}{[HA]}$
1.00	-161.6990	0.0	0.2824	0.3041	1.0768	0.0
2.50	-154.5700	0.2008	0.2849	0.3056	1.0727	6.7235e-3
3.00	-145.7100	0.6000	0.2859	0.3037	1.0623	0.0247
3.25	-139.0500	1.1330	0.2816	0.2948	1.0471	0.0518
3.50	-133.9300	1.8675	0.2858	0.2940	1.0286	0.0869
3.75	-128.8200	3.3688	0.2814	0.2791	0.9918	0.1643
4.00	-125.3300	5.8005	0.2883	0.2700	0.9366	0.3032
4.25	-121.9300	13.8568	0.2850	0.2430	0.8526	0.5929
4.50	-120.8830	22.3895	0.2799	0.2223	0.7940	0.8847
4.75	-120.5400	27.8101	0.2893	0.2014	0.6961	1.7177
5.00	-119.7300	62.6403	0.2814	0.1788	0.6351	2.7493
7.00	-119.0600	N/A	0.2825	0.1340	0.4745	N/A

(b) 3.05 M Methanol

Apparent pH (electrode)	chemical shift (δ) (ppm)	$\frac{[F^-]}{[HF]}$	*o*-HBA Isosbestic point absorbance @ 300 nm	*o*-HBA absorbance @ 310 nm	Normalized absorbance ($\frac{A_{310}}{A_{300}}$)	$(\frac{A_{obs}-A_{acid}}{A_{basic-}-A_{acid}}) = \frac{[A^-]}{[HA]}$
1.00	-163.1807	0.0	0.4909	0.4415	0.8993	0.0
1.50	-162.7363	0.0108	0.4596	0.4113	0.8949	0.0135
2.00	-161.7032	0.0367	0.4577	0.4042	0.8833	0.0514
2.25	-160.6768	0.0639	0.4624	0.4026	0.8706	0.0957
2.50	-159.0124	0.1111	0.4464	0.3801	0.8516	0.1699
2.75	-156.2050	0.2009	0.4565	0.3746	0.8206	0.3153
3.00	-152.1081	0.3616	0.4603	0.3584	0.7786	0.5821
3.25	-148.9765	0.5167	0.4480	0.3360	0.7499	0.8355
3.50	-141.6229	1.0707	0.4332	0.2990	0.6902	1.7576
4.00	-131.6866	3.0883	0.4365	0.2737	0.6269	4.8850
4.50	-125.1516	10.3822	0.4364	0.2569	0.5888	17.6123
7.00	-121.4887	N/A	0.4922	0.2811	0.5711	N/A
Apparent pH (electrode)	chemical shift (δ) (ppm)	$\frac{[F^-]}{[HF]}$	*p*-HBA Isosbestic point absorbance @ 247 nm	*p*-HBA absorbance @ 261 nm	Normalized absorbance ($\frac{A_{310}}{A_{300}}$)	$(\frac{A_{obs}-A_{acid}}{A_{basic-}-A_{acid}}) = \frac{[A^-]}{[HA]}$
1.00	-163.1807	0.0	0.6774	0.7361	1.0867	0.0
2.50	-159.0124	0.1111	0.6240	0.6763	1.0838	4.6773e-3
3.00	-152.1081	0.3616	0.6109	0.6587	1.0782	0.0137
3.25	-148.9765	0.5167	0.6367	0.6840	1.0742	0.0204
3.50	-141.6229	1.0707	0.6209	0.6573	1.0587	0.0469
3.75	-136.1479	1.8441	0.6667	0.6945	1.0417	0.0775
4.00	-131.6866	3.0883	0.6282	0.6362	1.0129	0.1339
4.25	-127.6415	5.7761	0.5988	0.5754	0.9609	0.2518
4.50	-125.1516	10.3822	0.6539	0.5820	0.8900	0.4592
4.75	-124.2195	14.2673	0.5870	0.4958	0.8447	0.6318
5.00	-122.9907	26.7577	0.6370	0.4757	0.7468	1.1919
7.00	-121.4887	N/A	0.6293	0.2904	0.4616	N/A

(c) 6.02 M Methanol						
Apparent pH (electrode)	chemical shift (δ) (ppm)	$\frac{[F^-]}{[HF]}$	*o*-HBA Isosbestic point absorbance @ 300 nm	*o*-HBA absorbance @ 310 nm	Normalized absorbance ($\frac{A_{310}}{A_{300}}$)	$(\frac{A_{obs}-A_{acid}}{A_{basic-}-A_{acid}}) = \frac{[A^-]}{[HA]}$
1.00	-164.1490	0.0	0.7092	0.6438	0.9078	0.0
1.50	-163.6900	0.0113	0.7096	0.6396	0.9014	0.0198
2.00	-162.7580	0.0352	0.7112	0.6336	0.8909	0.0539
2.25	-161.6790	0.0642	0.7072	0.6204	0.8772	0.1021
2.50	-159.9290	0.1149	0.6569	0.5563	0.8470	0.2256
2.75	-156.7120	0.2220	0.7060	0.5752	0.8148	0.3919
3.00	-153.8630	0.3356	0.6994	0.5484	0.7841	0.5983
3.25	-148.5200	0.6176	0.7016	0.5137	0.7322	1.1345
3.50	-142.7800	1.0923	0.6884	0.4724	0.6862	2.0377
4.00	-132.8800	3.2356	0.6898	0.4294	0.6225	6.3309
4.50	-126.7990	10.4242	0.6862	0.4051	0.5904	24.5400
7.00	-123.2160	N/A	0.6889	0.3978	0.5775	N/A
Apparent pH (electrode)	chemical shift (δ) (ppm)	$\frac{[F^-]}{[HF]}$	*p*-HBA Isosbestic point absorbance @ 247 nm	*p*-HBA absorbance @ 261 nm	Normalized absorbance ($\frac{A_{310}}{A_{300}}$)	$(\frac{A_{obs}-A_{acid}}{A_{basic-}-A_{acid}}) = \frac{[A^-]}{[HA]}$
1.00	-164.1490	0.0	0.5227	0.5700	1.0905	0.0
2.50	-159.9290	0.1149	0.4629	0.5069	1.0949	-6.8651e-3
3.00	-153.8630	0.3356	0.5011	0.5442	1.0861	7.1036e-3
3.25	-148.5200	0.6176	0.5018	0.5422	1.0806	0.0161
3.50	-142.7800	1.0923	0.5089	0.5438	1.0688	0.0358
3.75	-137.3500	1.8961	0.5524	0.5786	1.0474	0.0736
4.00	-132.8800	3.2356	0.5802	0.5944	1.0245	0.1174
4.25	-129.4500	5.5661	0.5813	0.5698	0.9802	0.2128
4.50	-126.7990	10.4242	0.5267	0.4777	0.9069	0.4127
4.75	-125.3840	17.8805	0.5681	0.4702	0.8277	0.7186
5.00	-124.4250	32.8569	0.5679	0.4178	0.7357	1.2966
7.00	-123.2160	N/A	0.5868	0.2711	0.4620	N/A

(d) 8.89 M Methanol						
Apparent pH (electrode)	chemical shift (δ) (ppm)	$\frac{[F^-]}{[HF]}$	*o*-HBA Isosbestic point absorbance @ 300 nm	*o*-HBA absorbance @ 310 nm	Normalized absorbance ($\frac{A_{310}}{A_{300}}$)	$(\frac{A_{obs}-A_{acid}}{A_{basic-}-A_{acid}}) = \frac{[A^-]}{[HA]}$
1.00	-165.1242	0.0	0.4884	0.4481	0.9174	0.0
1.50	-164.8396	7.1512e-3	0.6973	0.6377	0.9144	8.9496e-3
2.00	-164.6150	0.0129	0.4690	0.4264	0.9091	0.0250
2.25	-164.1012	0.0262	0.4756	0.4280	0.9001	0.0540
2.50	-163.1457	0.0519	0.4829	0.4299	0.8902	0.0874
2.75	-161.5706	0.0973	0.4933	0.4274	0.8663	0.1775
3.00	-159.1090	0.1766	0.4826	0.4030	0.8350	0.3212
3.25	-156.5033	0.2740	0.4697	0.3770	0.8027	0.5117
3.50	-152.4380	0.4631	0.4904	0.3694	0.7533	0.9392
4.00	-140.5532	1.5841	0.4671	0.3104	0.6644	2.9481
4.50	-134.2190	3.3678	0.4746	0.2940	0.6196	7.2609
7.00	-125.0423	N/A	0.4903	0.2837	0.5786	N/A
Apparent pH (electrode)	chemical shift (δ) (ppm)	$\frac{[F^-]}{[HF]}$	*p*-HBA Isosbestic point absorbance @ 247 nm	*p*-HBA absorbance @ 261 nm	Normalized absorbance ($\frac{A_{310}}{A_{300}}$)	$(\frac{A_{obs}-A_{acid}}{A_{basic-}-A_{acid}}) = \frac{[A^-]}{[HA]}$
1.00	-165.1242	0.0	0.6612	0.7259	1.0978	0.0
2.50	-163.1457	0.0519	0.6656	0.7295	1.0960	2.8789e-3
3.00	-159.1090	0.1766	0.6660	0.7273	1.0920	9.2273e-3
3.25	-156.5033	0.2740	0.6276	0.6872	1.0949	4.5951e-3
3.50	-152.4380	0.4631	0.6859	0.7489	1.0918	9.5462e-3
3.75	-147.2899	0.8016	0.7261	0.7862	1.0827	0.0245
4.00	-140.5532	1.5841	0.6282	0.6732	1.0716	0.0435
4.25	-137.4839	2.2216	0.6978	0.7363	1.0551	0.0727
4.50	-134.2190	3.3678	0.6424	0.6635	1.0329	0.1150
4.75	-131.1497	5.5628	0.7378	0.7380	1.0003	0.1833
5.00	-129.1595	8.7352	0.6386	0.6076	0.9515	0.3029
7.00	-125.0423	N/A	0.6903	0.3235	0.4686	N/A

(e) 11.63 M Methanol						
Apparent pH (electrode)	chemical shift (δ) (ppm)	$\frac{[F^-]}{[HF]}$	*o*-HBA Isosbestic point absorbance @ 300 nm	*o*-HBA absorbance @ 310 nm	Normalized absorbance ($\frac{A_{310}}{A_{300}}$)	$(\frac{A_{obs}-A_{acid}}{A_{basic-}-A_{acid}}) = \frac{[A^-]}{[HA]}$
1.00	-166.6160	0.0	0.3961	0.3685	0.9304	0.0
1.50	-166.5160	2.5333e-3	0.3790	0.3516	0.9277	8.0334e-3
2.00	-166.1030	0.0131	0.3960	0.3651	0.9220	0.0251
2.25	-165.3910	0.0319	0.3925	0.3576	0.9111	0.0597
2.50	-165.1570	0.0383	0.3775	0.3418	0.9054	0.0787
2.75	-164.0160	0.0703	0.3833	0.3403	0.8879	0.1415
3.00	-161.6060	0.1449	0.3798	0.3235	0.8517	0.2982
3.25	-158.0870	0.2747	0.3789	0.3049	0.8048	0.5789
3.50	-154.6860	0.4316	0.3810	0.2918	0.7657	0.9259
4.00	-143.9800	1.3364	0.3805	0.2556	0.6717	3.0817
4.50	-134.4800	4.3205	0.3740	0.2298	0.6145	11.8317
7.00	-127.0420	N/A	0.3852	0.2264	0.5878	N/A
Apparent pH (electrode)	chemical shift (δ) (ppm)	$\frac{[F^-]}{[HF]}$	*p*-HBA Isosbestic point absorbance @ 247 nm	*p*-HBA absorbance @ 261 nm	Normalized absorbance ($\frac{A_{310}}{A_{300}}$)	$(\frac{A_{obs}-A_{acid}}{A_{basic-}-A_{acid}}) = \frac{[A^-]}{[HA]}$
1.00	-166.6160	0.0	0.5157	0.5675	1.1005	0.0
3.25	-158.0870	0.2747	0.5328	0.5852	1.0982	5.1772e-3
3.50	-154.6860	0.4316	0.5399	0.5920	1.0965	7.8178e-3
3.75	-149.1700	0.7884	0.5390	0.5883	1.0913	0.0161
4.00	-143.9800	1.3364	0.5353	0.5779	1.0795	0.0356
4.25	-139.2400	2.2443	0.5352	0.5696	1.0642	0.0620
4.50	-134.4800	4.3205	0.5501	0.5667	1.0302	0.1257
4.75	-131.8990	7.1478	0.5371	0.5304	0.9874	0.2176
5.00	-129.7600	13.5600	0.5370	0.4935	0.9191	0.3999
7.00	-127.0420	N/A	0.5343	0.2474	0.4631	N/A

The normalized absorbance differences of *o*-HBA and *p*-HBA in urea and methanol-water mixtures were plotted against their measured $\frac{[F^-]}{[HF]}$ ratios. Figure 14 depicts the titration plots of *o*-HBA and *p*-HBA in water compared to 5.98 M urea and 11.63 M methanol.

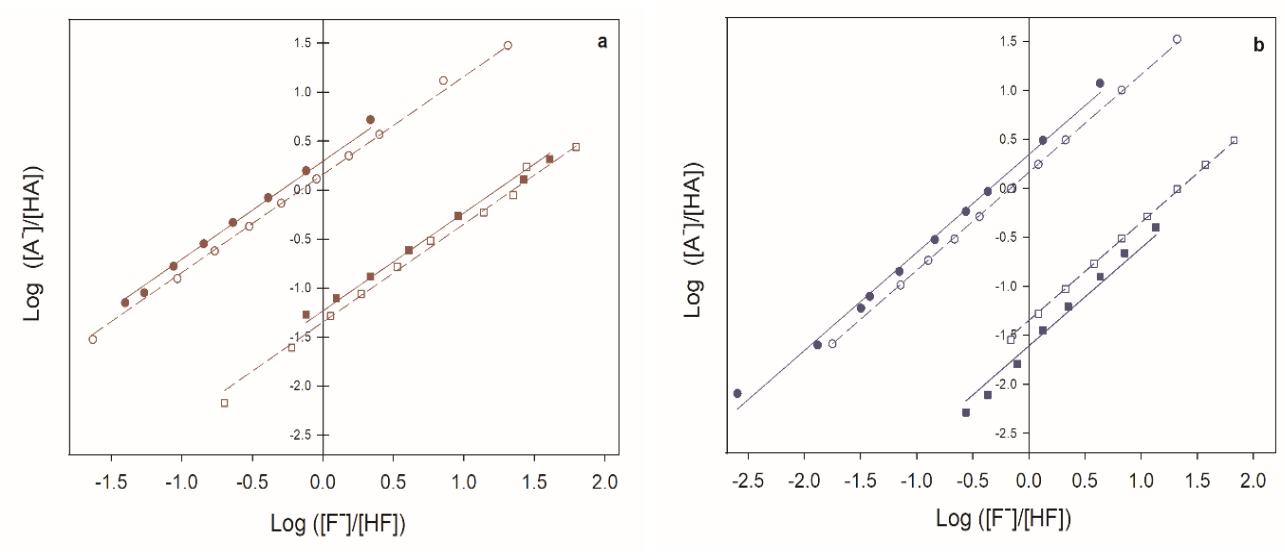

Figure 14. Spectrophotometric titration plots of 100 uM *o*-HBA (circles) and 25 uM *p*-HBA (squares), measured in: a) pure water (empty symbols) and 5.98 M urea (filled symbols), b) pure water (empty symbols) and 11.63 M methanol (filled symbols).

As it can be seen in Fig. 14, the pH dependence of both acids follows Eq-24 and Eq-25 closely, allowing us to determine ($\mathrm{p}K_{HF}^{apparent} - \mathrm{p}K_{HA}^{apparent}$) for both acids at various urea and methanol concentrations and have compiled them in Table 6. The effect of urea addition upon the *o*-HBA intramolecular H-bond strength (as represented by $K_H^{apparent}$) can be quantified by the following subtraction:

$$logK_H^{apparent} = \left(\mathrm{p}K_{HF}^{apparent} - \mathrm{p}K_{o-HBA}^{apparent}\right) - \left(\mathrm{p}K_{HF}^{apparent} - \mathrm{p}K_{p-HBA}^{apparent}\right)$$

$$= -logK_{p-HBA} - log\frac{\gamma_{p-HBA}}{\gamma_{p-BA^-}} + logK_{o-HBA} + log\frac{\gamma_{o-HBA}}{\gamma_{o-BA^-}}$$

$$= logK_H - log\frac{\gamma_{p-HBA}}{\gamma_{p-BA^-}} + log\frac{\gamma_{o-HBA}}{\gamma_{o-BA^-}}$$

$$\approx logK_H + log\frac{\gamma_{p-BA^-}}{\gamma_{o-BA^-}} \qquad (26)$$

K_H represents the H-bond strength between the carboxylate and hydroxyl groups of *o*-HBA measured in pure water; the final approximation can be applied because the H-bond between the protonated carboxylate and hydroxyl groups is weak [103]. Table 6 reports the measured Log K_H^{app} of *o*-HBA in urea-water mixtures and methanol-water mixtures.

Table 6. Reported Log K_H^{app} values of *o*-HBA and *p*-HBA in (a) urea-water mixtures and (b) methanol-water mixtures.

(a)

[Urea] (M)	$pK_{HF}^{app} - pK_{o-HBA}^{app}$	$pK_{HF}^{app} - pK_{p-HBA}^{app}$	Log K_H^{app}
0.0000	0.16 ± 0.01	-1.35 ± 0.01	1.51 ± 0.01
2.0692	0.19 ± 0.02	-1.28 ± 0.03	1.47 ± 0.04
3.9820	0.27 ± 0.01	-1.21 ± 0.03	1.48 ± 0.03
5.9806	0.29 ± 0.02	-1.23 ± 0.02	1.52 ± 0.03

(b)

[Methanol] (M)	$pK_{HF}^{app} - pK_{o-HBA}^{app}$	$pK_{HF}^{app} - pK_{p-HBA}^{app}$	Log K_H^{app}
0.0000	0.16 ± 0.01	-1.35 ± 0.01	1.51 ± 0.01
3.0593	0.19 ± 0.01	-1.37 ± 0.01	1.56 ± 0.01
6.0218	0.26 ± 0.01	-1.47 ± 0.03	1.73 ± 0.03
8.8876	0.26 ± 0.02	-1.55 ± 0.04	1.81 ± 0.04
11.6292	0.34 ± 0.02	-1.61 ± 0.03	1.95 ± 0.04

In Fig. 15 we have plotted $logK_H^{app}$ as a function of urea and methanol concentration. The magnitude of K_H^{app} is clearly unaffected by urea addition, demonstrating no preferential interaction[107] between urea and *o*-HBA. Urea addition therefore, has no effect upon the intramolecular H-bond formed between the carboxylate and hydroxyl groups of *o*-HBA. **Thus, it can be said that urea addition has no significant effect upon the intramolecular H-bonds of solutes dissolved in water.** In contrast, Fig. 15 demonstrates that methanol addition significantly increases the magnitude of K_H^{app}. This is most likely due to the fact at the methanol concentrations

studied, the dominant effect of methanol addition to water is to lower solvent H-bond donation, thereby reducing the solvent's ability to compete with intramolecular H-bonding.

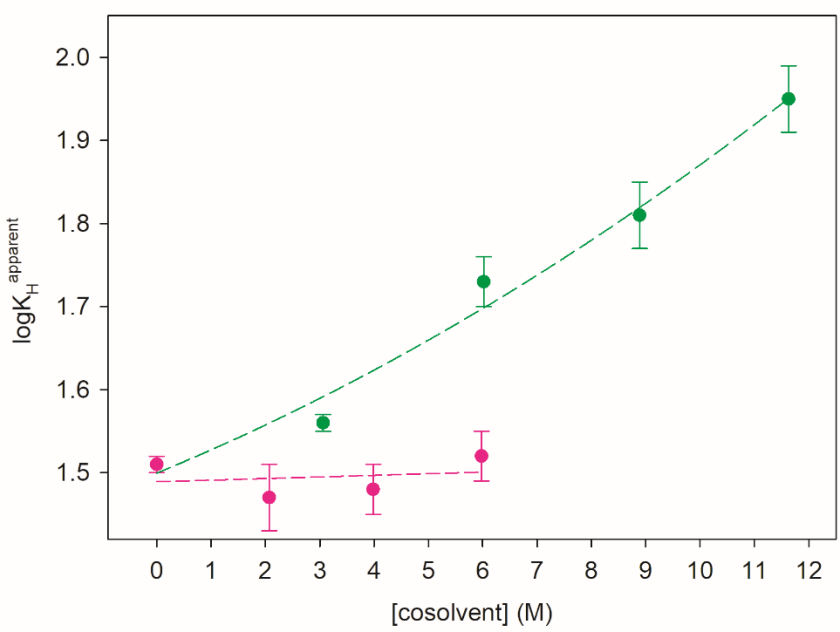

Figure 15. Effects of urea (pink circles) and methanol (green circles) addition upon the intramolecular hydrogen bond strength of *o*-HBA in water.

References

101. Hermans, J.; Leach, S. J.; Scheraga, H. A., Thermodynamic Data from Difference Spectra.1,2 II. Hydrogen Bonding in Salicylic Acid and its Implications for Proteins. *Journal of the American Chemical Society.* (1963); *85* (10), 1390-1395.

102. Luo, P., Baldwin, R.L. Mechanism of helix induction by trifluoroethanol: A framework for extrapolating the helix-forming properties of peptides from trifluoroethanol/water mixtures back to water. *Biochemistry.* **(**1997); *36*(27), 8413-8421.

103. Shan, S.O.; Herschlag, D., The change in hydrogen bond strength accompanying charge rearrangement: Implications for enzymatic catalysis. *Proceedings of the National Academy of Sciences.* (1996); *93* (25), 14474-14479.

104. Rondinini, S. pH measurements in non-aqueous and aqueous–organic solvents – definition of standard procedures. *Analytical and Bioanalytical Chemistry.* (2002); *374* (5), 813-816.

105. Deleebeeck, L., Snedden, A., Nagy, D., Szilágyi Nagyné, Z., Roziková, M., Vičarová, M., Heering, A., Bastkowski, F., Leito, I., Quendera, R,; Cabral, V., Stoica, D., Unified pH Measurements of Ethanol, Methanol, and Acetonitrile, and Their Mixtures with Water. *Sensors.* (2021); *21* (11).

106. Frohliger, J. O., Dziedzic, J. E., Steward, O. W. Simplified spectrophotometric determination of acid dissociation constants. *Analytical Chemistry.* (1970); *42* (11), 1189-1191.

107. Pegram, L. M.; Wendorff, T.; Erdmann, R.; Shkel, I.; Bellissimo, D.; Felitsky, D. J.; Record, M. T., Jr., Why Hofmeister effects of many salts favor protein folding but not DNA helix formation. *Proceedings of the National Academy of Sciences.* (2010); *107* (17), 7716-7721.

108. Rossky, P.J. Protein denaturation by urea: slash and bond. *Proceedings of the National Academy of Sciences*. (2008); 105(44):16825-16826.

Part III: Determination of the Effects of the addition of Urea on the Solubility of a Model Compound System

3.3.1. Analyzing the Effects of Co-solvents on Acetaminophen and 4-tertbutylphenol Solubility

In this work, we study the effects of urea and acetonitrile upon the solvation of amide moieties by comparing their effects upon the solubilities of acetaminophen and 4-tertbutylphenol (Fig. 16) in water. Since these compounds are different only in the functional groups attached to the phenol; we can associate relative changes in their solubility to these structural constituents. Both of these molecules are sparingly soluble in water [109,110], allowing their solvation to be partitioned into two thermodynamic steps: 1) cavitation, 2) solvent-solute interactions [61, 111-114]. Consequently, any change in their solubility in water upon urea addition results from the net effect of urea upon these two processes.

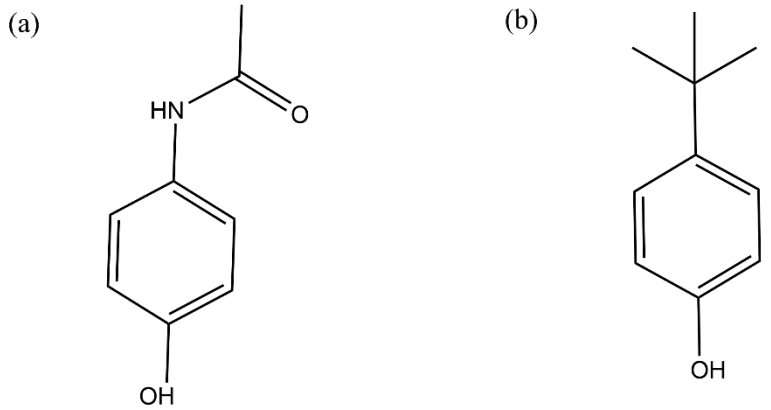

Figure 16. Structure of (a) acetaminophen (b) 4-tertbutylphenol.

Theoretical studies have shown that adding urea leads to an increase in the free energy of cavitation, emphasizing the role of increased solvent-solute interactions in the denaturation process [61, 115]. Relative to 4-tertbutylphenol, acetaminophen can H-bond with solvent in a larger number of modalities, and this is reflected in its higher water solubility. If, however, urea denaturation is only effected through van der Waals dispersion interactions, then the urea gradient of solvent-

solute interactions these two compounds should be very close (these two molecules differ by only one Dalton in mass).

3.3.2. Determination of Acetaminophen and 4-tertbutylphenol Extinction Coefficients

Figure 17 depicts the absorbance spectra of acetaminophen and 4-tertbutylphenol. The extinction coefficients of acetaminophen at 260 nm and 4-tertbutylphenol at 275 nm were determined to be (3237 ± 95) and (1523 ± 26) $Lmol^{-1}cm^{-1}$ respectively. (Fig. 18).

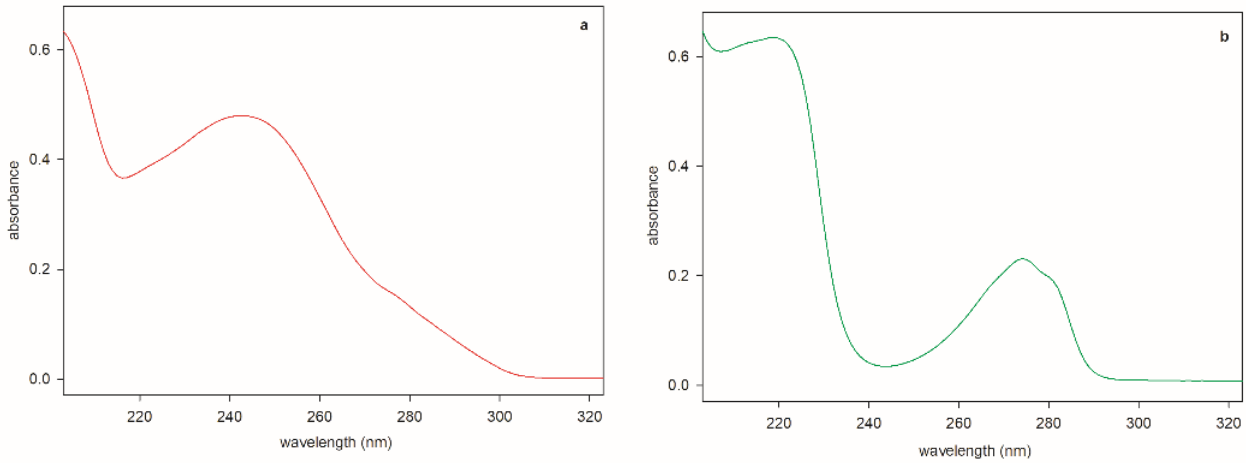

Figure 17. Absorbance spectra of (a) 150 µM acetaminophen and (b) 150 µM 4-tertbutylphenol in pure water.

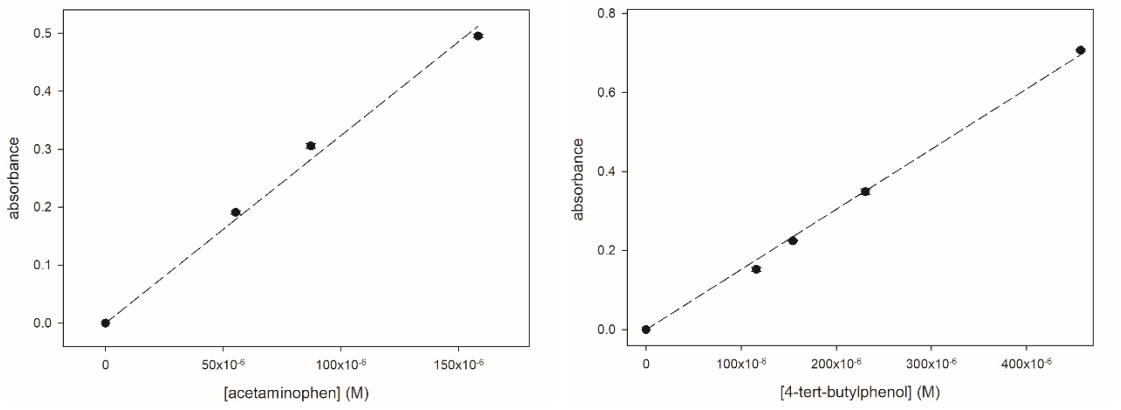

Figure 18. Calibration curves for the determination of the molar absorptivity coefficients of (a) acetaminophen and (b) 4-tertbutylphenol in pure water.

3.3.3. How do we measure the effects of Urea on the Solvation of Amide Units?

The solubilities of acetaminophen and 4-tertbutylphenol in urea-water and acetonitrile-water mixtures were measured spectrophotometrically as seen in Table 7, and the effect of these co-solvents on their solvation energies are visually depicted in Fig. 19.

Table 7 (a-b): Solubilities (S) of acetaminophen (ACT) and 4-tertbutylphenol (TBP) in (a) urea-water and (b) acetonitrile-water mixtures.

(a)

[Urea] (M)	Solubility, S_{ACT} (g/L)	[Urea] (M)	S_{TBP} (g/L)
0.0000	16.98 ± 1.16	0.0000	0.36 ± 0.06
1.4165	21.25 ± 0.34	1.4160	0.46 ± 0.08
3.1423	25.06 ± 0.76	2.8430	0.57 ± 0.34
5.6758	31.64 ± 0.25	5.3110	1.00 ± 0.03
7.0836	34.26 ± 0.67	0.0000	0.33 ± 0.07
0.0000	18.33 ± 2.15	1.4160	0.50 ± 0.09
1.4757	22.25 ± 2.46	2.8430	0.56 ± 0.06
3.0825	26.45 ± 2.53	5.3110	0.81 ± 0.14
5.4500	32.46 ± 1.61	0.0000	0.41 ± 0.23
7.0220	35.22 ± 0.89	1.4165	0.61 ± 0.16
0.0000	20.30 ± 0.95	3.1423	0.72 ± 0.01
1.7700	25.63 ± 0.77	5.6758	1.10 ± 0.07
3.6800	28.40 ± 0.94	7.0836	1.38 ± 0.04
5.4900	34.37 ± 0.84		
0.0000	17.71 ± 1.06		
1.0024	19.59 ± 1.17		
2.0692	23.25 ± 0.63		
3.2620	25.19 ± 0.61		
4.2830	27.64 ± 0.52		
5.1899	31.57 ± 0.07		
6.2680	33.16 ± 0.13		

(b)

[Acetonitrile] (M)	S_{ACT} (g/L)	[Acetonitrile] (M)	S_{TBP} (g/L)
0.0000	20.12 ± 1.56	0.0000	0.52 ± 0.06
2.3900	33.82 ± 0.58	1.1900	0.88 ± 0.06
3.5340	39.34 ± 0.67	2.3900	1.08 ± 0.06
4.6700	39.80 ± 0.29	3.5340	1.25 ± 0.08
6.8550	40.69 ± 1.10	4.6700	1.27 ± 0.07
		6.8550	1.32 ± 0.08

It can be clearly seen that both urea and acetonitrile addition increases the solubility of these two molecules in a monotonic fashion that can be adequately correlated with polynomial or hyperbolic expressions.

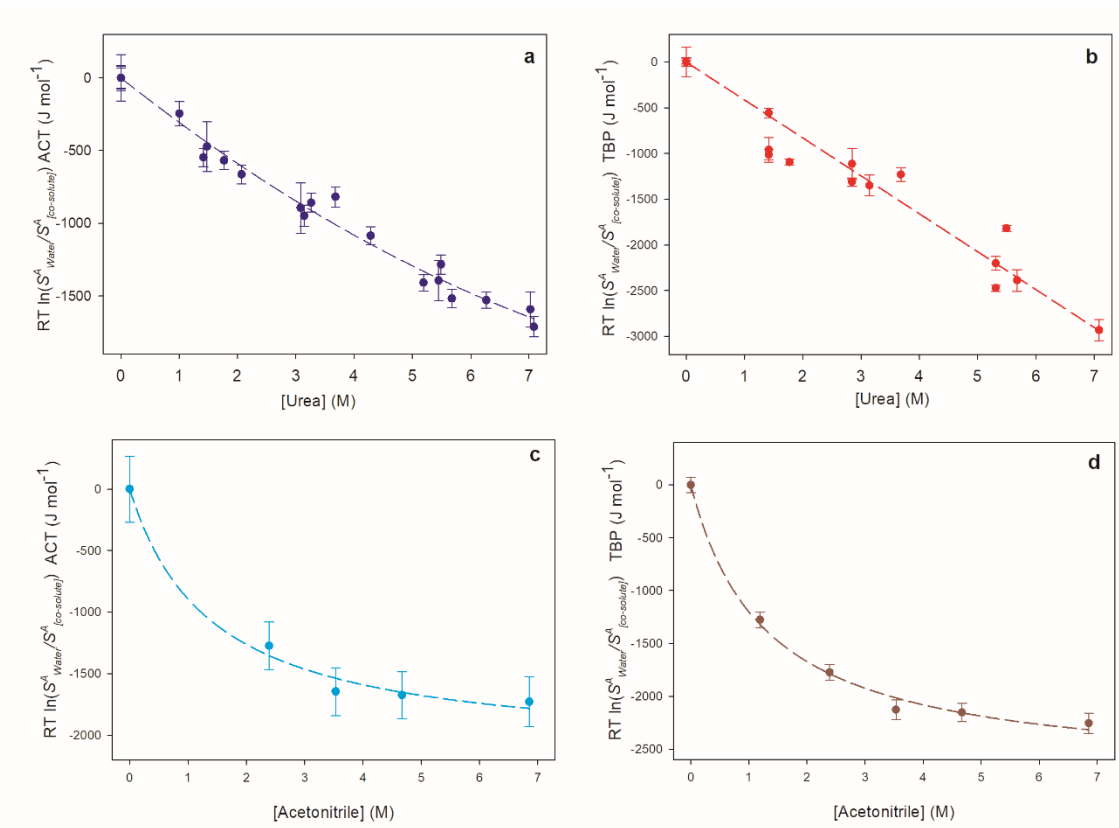

Figure 19. Effects of urea and acetonitrile addition upon the measured solubilities of acetaminophen (panels a and c) and 4-tertbutylphenol (panels b and d). Dashed lines represent the best correlation curves fitting the experimental data. The equations of the correlation curves are: a) $-317.7 \times [Urea] + 11.85 \times [Urea]^2$, b) $-414.8 \times [Urea]$, c) $\frac{-2147.2 \times [ACN]}{1.405 + [ACN]}$ and d) $\frac{-2753.4 \times [ACN]}{1.296 + [ACN]}$.

The effect of co-solvent addition upon the solubility of a given compound in water can be expressed as [116]:

$$ln\frac{s^A_{water}}{s^A_{[co-solvent]}} = \frac{\left[\mu^A_{[co-solvent]} - \mu^A_{water}\right]}{RT} \quad (27)$$

Where s^A_{water} is the solubility of compound A in pure water and $s^A_{[co-solvent]}$ is the solubility of A in a given concentration of co-solvent, μ is respectively, the standard chemical of compound A as defined by Ben-Naim[116] (the reversible work required to transfer a mole of solute molecules from the ideal gas phase to the liquid phase at constant temperature and pressure) measured in pure water and given concentration of co-solvent.

For dilute solutions, the solvation of a molecule in water can be approximated as the sum of two thermodynamic processes[111-113, 117]: first, the creation of a cavity large enough to accommodate the molecule; second, turning on solvent-solute interactions. In this case μ can be defined as:

$$\mu = \Delta G_c + E_i = \Delta G_c + E_{VdW} + E_{H-bond,donation} + E_{H-bond,acceptance} \quad (28)$$

In which ΔG_c is the solvent cavitation free energy and E_i is the aggregate sum of the solvent-solute interaction enthalpies. For our analysis, we have partitioned E_i into 3 terms: E_{VdW} representing solvent-solute van der Waals interaction enthalpy, $E_{H-bond,donation}$ solvent-to-solute H-bond donation interaction enthalpy, $E_{H-bond,acceptance}$ solvent-from-solute H-bond accepting interaction enthalpy. Substituting Eq-27 into Eq-28 yields:

$$RT \times ln\frac{s^A_{water}}{s^A_{[co-solvent]}} = \Delta\Delta G_c + \Delta E_{VdW} + \Delta E_{H-bond,donation} + \Delta E_{H-bond,acceptance} \quad (29)$$

$\Delta\Delta G_c$, ΔE_{VdW}, $\Delta E_{H-bond,donation}$ and $\Delta E_{H-bond,acceptance}$ are the differences between solvent cavitation free energy, solvent-solute van der Waals interaction energy, solvent-to-solute

H-bond donation interaction energy, and solvent-from-solute H-bond acceptance interaction energy measured in pure water and binary aqueous mixture at a given co-solvent concentration.

Calculating solvent cavitation free energies for aqueous systems involves modeling solvent and solute molecules as hard spheres and using experimental data at key points when applying theory[118]. The resulting calculations are therefore very sensitive towards the quality of experimental data used and the values chosen for hard sphere diameters. These calculations become even more complicated in the case of mixed solvents. Our choice of acetaminophen and 4-tertbutylphenol was done purposely: their molecular diameters are close (van der Waals diameters of 6.46 Å for acetaminophen and 6.72 Å for 4-tertbutylphenol calculated using the method of Bondi[119]) and their geometries are similar. Co-solvent effects upon the cavitation free energy ($\Delta\Delta G_c$), should therefore be very close for these two solutes regardless of the method used for calculation.

3.3.4. Calculating the Solvent Cavitation Free Energy using Scaled Particle Theory (SPT)

Changes in cavitation free energy due to co-solvent addition ($\Delta\Delta G_c$) may be calculated using scaled particle theory[61,112,120,121] by treating binary solvent systems as "uniform solvent systems" having a single mean molar volume and a single mean hard-sphere diameter (Fig. 20) [61,120,121].

$$\frac{\Delta G}{RT} = K_0 + K_1\frac{\sigma_2}{\sigma_1} + K_2\left(\frac{\sigma_2}{\sigma_1}\right)^2 + K_3\left(\frac{\sigma_2}{\sigma_1}\right)^3 \qquad (30)$$

σ_1 and σ_2 are the hard-sphere diameters of the solvent and solute, $K_0 = -\ln(1-\xi)$, $K_1 = u = \frac{3\xi}{1-\xi}$, $K_2 = \frac{u(u+2)}{2}$, $K_3 = \frac{\xi P V_1}{RT}$, $\xi = \frac{\pi\sigma_1^3 N_{Av}}{6V_1}$; P is the pressure, T is temperature, R is the gas constant, N_{Av} is the Avogadro number and V_1 is the solvent molar volume. We have calculated $\Delta\Delta G_c$ for both urea and acetonitrile addition using scaled-particle theory[61,112,120,121]. The molar volume of water is assumed to be 18.07 cm^3/mol,[61] molar volumes for mixed solvent systems were calculated from

literature values [122-124]. For solvent systems, σ_2 values have been set to the following: water (2.75 Å) [61]; urea (4.6Å) and acetonitrile (4.5Å), these values were calculated using their van der Waals radii[119,125-126]. For binary solvent mixtures, σ_1 was calculated using the equation $\sigma_{mixture} = (1 - x_{co-solvent})\sigma_{water} + x_{co-solvent}\sigma_{co-solvent}$, the mole fraction of the co-solvent ($x_{co-solvent}$) was calculated using experimental volumetric properties[122]. For the solute, σ_2 was calculated to be equal to the diameter of a sphere having an equal volume to the solute van der Waals volume as calculated using the method[127] of Bondi. The parameters used in this SPT analysis are presented in Table 8. As seen in Fig. 21, our calculations show that co-solvent addition has essentially the same effect on solvent cavitation for both molecules:

$$(\Delta\Delta G_c)_{acetaminophen} - (\Delta\Delta G_c)_{4-tertbutylphenol} \approx 0 \quad (31)$$

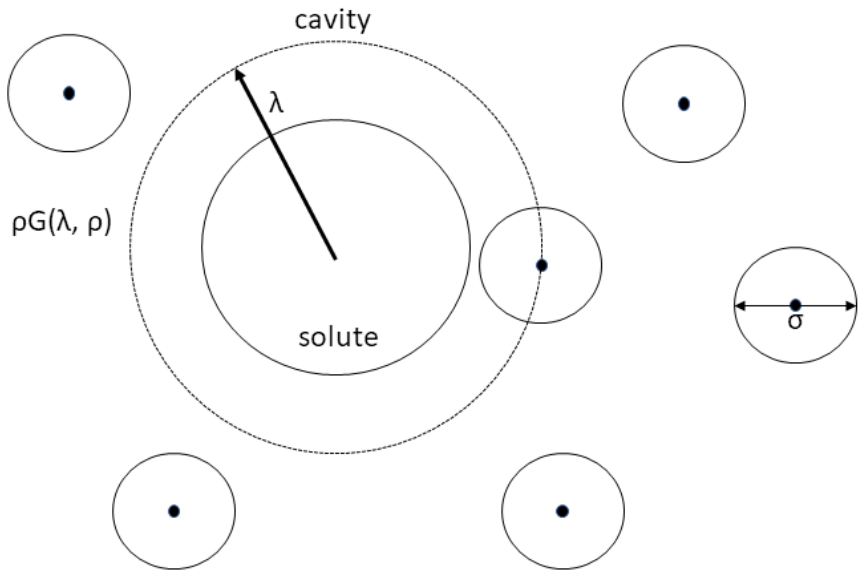

Figure 20. Illustration of the interaction between a cavity of radius λ and spherical hard particles of diameter σ. The centers of the particles are excluded from the dashed volume of the cavity. The solid sphere inside the cavity is the equivalent hard sphere solute of radius λ - σ/2. The local density of hard particle centers in contact with the cavity surface is denoted by ρG(λ, ρ). Adapted from Corti (2004) [128].

Table 8. Parameters required or calculated for scaled particle theory analysis of the solubility data (abbreviations: ACT (acetaminophen); TBP (4-tertbutylphenol) [61, 112, 119-127].

[Urea] (M)	σ_{UREA} (Å)	Packing density (ξ) (m^3)	$\Delta\Delta G_{cav\text{-}ACT}$ ($Jmol^{-1}$)	$-RTln(S/S_0)_{ACT}$ ($Jmol^{-1}$)	$\Delta Ei_{\text{-}ACT}$ ($Jmol^{-1}$)	$\Delta\Delta G_{cav\text{-}TBP}$ ($Jmol^{-1}$)	$-RTln(S/S_0)_{TBP}$ ($Jmol^{-1}$)	$\Delta E_{a\text{-}TBP}$ ($Jmol^{-1}$)
0.0000	2.7500	0.3619	0.0000	0.00 ± 156.97	0.00 ± 156.97	0.0000	0.00 ± 490.88	0.00 ± 490.88
1.0000	2.7835	0.3656	38.1729	-315.14 ± 159.61	-353.3129 ± 159.61	38.4132	-468.38 ± 491.99	-506.79 ± 491.99
2.0000	2.8196	0.3698	114.9983	-603.95 ± 163.48	-718.9483 ± 163.48	118.2279	-911.59 ± 495.33	-1029.82 ± 495.33
3.0000	2.8582	0.3743	236.9441	-866.44 ± 165.38	-1103.3841 ± 165.38	246.4054	-1329.65 ± 501.03	-1576.05 ± 501.03
4.0000	2.8995	0.3792	410.6773	-1102.61 ± 164.76	-1513.2873 ± 164.76	430.1213	-1722.56 ± 508.70	-2152.68 ± 508.70
5.0000	2.9433	0.3845	643.1050	-1312.46 ± 163.62	-1955.5650 ± 163.62	676.8091	-2090.30 ± 518.68	-2767.11 ± 518.68
6.0000	2.9898	0.3902	941.4360	-1495.98 ± 166.51	-2437.4160± 166.51	994.2273	-2432.88 ± 529.96	-3427.10 ± 529.96
7.0000	3.0388	0.3963	1313.2644	-1653.19 ± 179.89	-2966.4544 ± 179.89	1390.5491	-2750.30 ± 543.32	-4140.85 ± 543.32
[ACN] (M)	σ_{ACN} (Å)	Packing density (ξ) (m^3)	$\Delta\Delta G_{cav\text{-}ACT}$ ($Jmol^{-1}$)	$-RTln(S/S_0)_{ACT}$ ($Jmol^{-1}$)	$\Delta Ei_{\text{-}ACT}$ ($Jmol^{-1}$)	$\Delta\Delta G_{cav\text{-}TBP}$ ($Jmol^{-1}$)	$-RTln\ (S/S_0)_{TBP}$ ($Jmol^{-1}$)	$\Delta E_{a\text{-}TBP}$ ($Jmol^{-1}$)
0.0000	2.7500	0.3629	0.0000	0.00 ± 268.52	0.0000 ± 268.52	0.0000	0.00 ± 187.13	0.00 ± 187.13
1.0000	2.7819	0.3640	-749.8470	-892.71 ± 341.63	-142.8630 ± 341.63	-808.9528	-1199.41 ± 141.02	-390.45 ± 141.02
2.0000	2.8169	0.3654	-1478.1580	-1261.10 ± 372.77	217.0580 ± 372.77	-1594.9008	-1670.94 ± 132.11	-76.04 ± 132.11
3.0000	2.8550	0.3672	-2169.4261	-1462.24 ± 405.58	707.1861 ± 405.58	-2341.1596	-1922.93 ± 179.95	418.23 ± 179.95
4.0000	2.8963	0.3694	-2809.6585	-1588.96 ± 450.19	1220.6985 ± 450.19	-3032.6771	-2079.75 ± 217.52	952.93 ± 217.53
5.0000	2.9408	0.3720	-3386.3237	-1676.10 ± 455.07	1710.2237 ± 455.07	-3655.9756	-2186.75 ± 253.86	1469.23 ± 253.86
6.0000	2.9884	0.3752	-3888.2058	-1739.72 ± 448.98	2148.4858 ± 448.98	-4198.9948	-2264.41 ± 244.54	1934.58 ± 244.54

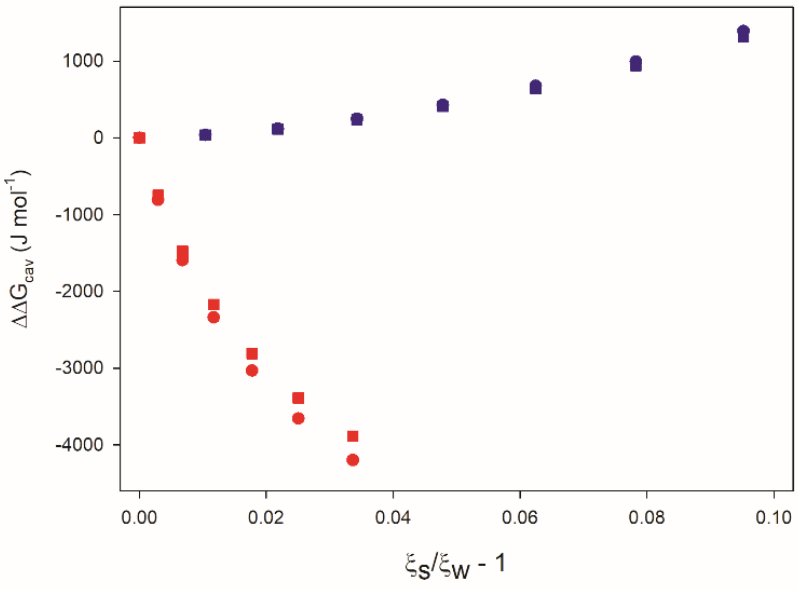

Figure 21. Effects of urea (blue) and acetonitrile (red) addition upon the cavitation free-energies of acetaminophen (squares) and 4-tertbutylphenol (circles), as a function of the change in packing density of the solvent system ξ.

3.3.5. Urea Solubilizes Aqueous Amide Bonds Through Enhanced van der Waals Interactions

Van der Waals interactions of nonpolar molecules with water solvent has been shown to be incremental [129]. If van der Waals interactions between acetaminophen and water are partitioned between the phenol and methyl-amide groups, while those of 4-tertbutylphenol are partitioned into the phenol and alkyl groups, we can write:

$$(\Delta E_{VdW})_{acetaminophen} - (\Delta E_{VdW})_{t-butylphenol} \approx (\Delta E_{VdW})_{methyl-amide} - (\Delta E_{VdW})_{t-butyl} \quad (32)$$

Solvent-solute van der Waals interaction energies between water and nonpolar molecules are suggested to be of the form $(E_{VdW})_{water} = -\mathrm{A}\rho$ where A is the van der Waals mean field coefficient and ρ is the solvent number density [130]. The value of the constant A has been approximately related to the geometric mean of pure solvent and pure solute fluid van der Waals mean-field parameters [130-131], redefining:

$$(E_{VdW})_{water} = -8\mathrm{R}\sqrt{\tau_u \tau_w d^3} \times \xi \quad (33)$$

Where R is the ideal gas constant, τ_u and τ_w are van der Waals attractive mean field coefficients of solute and solvent, d is the solvent-solute diameter ratio, and ξ is the solvent packing density as defined previously. If the addition of co-solvent does not significantly change the influence of long-range dispersive and multipolar intermolecular interactions and the "effective" solvent diameter (the product $\{\tau_w d^3\}$ does not change much), which is a reasonable assumption at low co-solvent concentrations, and the mixed solvent system is treated as a "uniform solvent system" having a single mean molar volume and a single mean hard-sphere diameter[61], Eq-33 can be used to estimate co-solvent effects upon the solvent-solute van der Waals interaction energies[61, 111, 117]:

$$\Delta E_{VdW} = E_{VdW}^{H_2O}\left(\frac{\xi^{[co-solvent]}}{\xi^{H_2O}} - 1\right) \quad (34)$$

ξ^{H_2O} and $\xi^{[co-solvent]}$ are the solvent packing densities of pure water and binary solvent mixtures as previously defined, $E_{VdW}^{H_2O}$ is the solvent-solute van der Waals interaction energy measured in water. Even though Eq-33, is just a "reasonable rough estimate" of van der Waals interactions, and its physical applicability to aqueous systems may be questioned [130], its modification Eq-34 has been shown to be useful in characterizing co-solvent effects upon solvent-solute van der Waals interactions[61,111,115,132,133]. This is probably because the parameter $E_{VdW}^{H_2O}$ has been empirically adjusted. Equation 32 can therefore be written as:

$$(\Delta E_{VdW})_{acetaminophen} - (\Delta E_{VdW})_{t-butylphenol} \approx (\Delta E_{VdW})_{methyl-amide} - (\Delta E_{VdW})_{t-butyl} =$$

$$\left(\frac{\xi^{[co-solvent]}}{\xi^{H_2O}} - 1\right) \times \left\{\left(E_{VdW}^{H_2O}\right)_{methylamide} - \left(E_{VdW}^{H_2O}\right)_{t-butyl}\right\} \quad (35)$$

Finally, the difference between co-solvents effects upon the solvent-solute H-bonding of acetaminophen and 4-tertbutylphenol can be represented by the following equation if the hydroxyl group of the two molecules are considered equivalent in terms of H-bonding:

$$\left(\Delta E_{H-bond,donation} + \Delta E_{H-bond,acceptance}\right)_{acetaminophen} - \left(\Delta E_{H-bond,donation} + \right.$$

$$\left.\Delta E_{H-bond,acceptance}\right)_{t-butylphenol} \approx \Delta E_{H-bond,donation}^{amide} + \Delta E_{H-bond,acceptance}^{amide} \quad (36)$$

If Equations 31, 35 and 36 are combined we obtain:

$$RT\left(ln\frac{s_{water}^{A}}{s_{[co-solvent]}^{A}}\bigg|_{acetaminophen} - ln\frac{s_{water}^{A}}{s_{[co-solvent]}^{A}}\bigg|_{t-butylphenol}\right) \approx \left(\frac{\xi^{[co-solvent]}}{\xi^{H_2O}} - 1\right) \times$$

$$\left\{\left(E_{VdW}^{H_2O}\right)_{methylamide} - \left(E_{VdW}^{H_2O}\right)_{t-butyl}\right\} + \Delta E_{H-bond,donation}^{amide} + \Delta E_{H-bond,acceptance}^{amide} = \Delta\psi \quad (37)$$

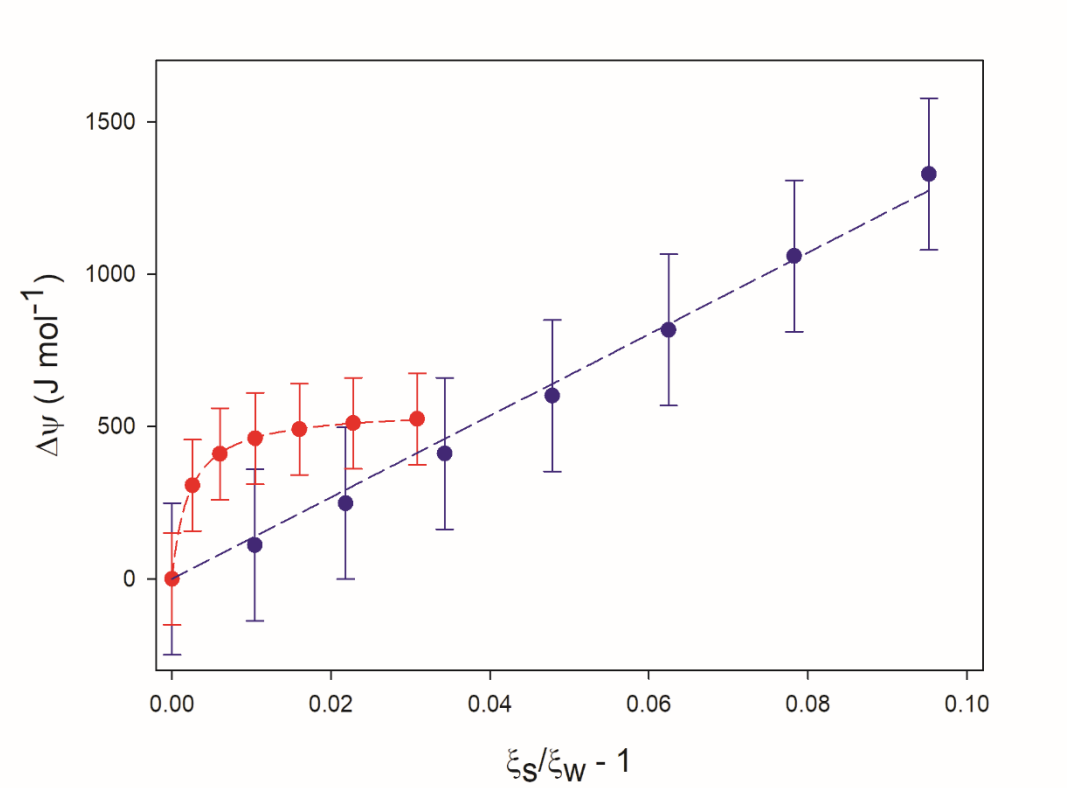

Figure 22. ΔΨ plotted as a function of the change in packing density of the solvent system for urea (blue) and acetonitrile (red).

In Fig. 22, we have plotted the effects of acetonitrile addition upon the solubilities of acetaminophen and 4-tertbutylphenol as represented by $\Delta\psi$ as a function of $\frac{\xi^{[co-solvent]}}{\xi^{H_2O}} - 1$. Clearly, $\Delta\psi$ does not linearly depend upon $\frac{\xi^{[co-solvent]}}{\xi^{H_2O}} - 1$. This non-linearity is consistent with our fluorescence results suggesting that acetonitrile addition affects solvent H-bonding. Initial addition of acetonitrile increases solvent packing (van der Waals interactions) and reduces solvent H-bond donation both leading to an increase in the initial slope of the $\Delta\psi$ plot. As concentrations of acetonitrile are increased, the solvent becomes a better H-bond acceptor. This favorable interaction causes a decrease in the slope of $\Delta\psi$ leading to a flattening of the curve. Thus, demonstrating that our analysis is sensitive towards changes in H-bonding.

In the case of urea addition to water, our fluorescence data show that urea's contributions to $\Delta E^{amide}_{H-bond,donation}$ and $\Delta E^{amide}_{H-bond,acceptance}$ are zero. Therefore, if changing solvent-solute van der Waals interactions is the only effect of urea addition, $\Delta\psi$ should show linear dependence upon urea-induced changes in solvent packing density. Figure 22 also plots $\Delta\psi$ as a function of $\left(\frac{\xi^{[co-solvent]}}{\xi^{H_2O}} - 1\right)$ for water-urea mixtures, where a linear plot is obtained. The slope of the plot obtained from the regression line is $\left(E^{H_2O}_{VdW}\right)_{amide} - \left(E^{H_2O}_{VdW}\right)_{t-butyl}$ = 13.4 ± 0.2 kJ M^{-1}. The results of most theoretical analysis suggest that van der Waals interactions between amides and water are similar to those of alkanes of the same size(134). Interestingly, the value of = 13.4 kJ M^{-1} is rather more than the differences between in water-alkane van der Waals interaction energies calculated for alkanes(129) having similar diameters (4.7Å and 5.2 Å are the estimated(119) van der Waals diameters of methylamide and tert-butyl groups). Perhaps, van der Waals interactions between water and the amide moiety are weaker than those with alkanes of similar size. That being said, if $\left(E^{H_2O}_{VdW}\right)_{t-butyl}$ is estimated to be -32.3 kJ mol^{-1}, the effect of urea addition upon the solvation of the amide group will be approximately $-18.9\left(\frac{\xi^{[co-solvent]}}{\xi^{H_2O}} - 1\right)$ kJ mol^{-1}. **Thus, confirming that the increase in solubility of amide moieties observed in urea solutions relative to pure water can be assigned to the increase in van der Waals solvent-solute interactions and not due to any enhancement of H-bonding interactions with the amide.**

References:

109. Granberg, R. A., Rasmuson, Å. C. Solubility of Paracetamol in Pure Solvents. *Journal of Chemical & Engineering Data.* (1999); *44* (6), 1391-1395.

110. Yalkowsky, S. H., He, Y.; Jain, P. *Handbook of aqueous solubility data*. 2nd ed.; CRC Press: Boca Raton, FL. (2010); p xii, 1608 p.

111. Graziano, G., On the Salting Out of Benzene by Alkali Chlorides. *J. Chem. Eng. Data.* (2009); *54* (2), 464-467.

112. Pierotti, R. A. A scaled particle theory of aqueous and nonaqueous solutions. *Chemical Reviews.* (1976); *76* (6), 717-726.

113. Lee, B., Solvent reorganization contribution to the transfer thermodynamics of small nonpolar molecules. *Biopolymers***.** (1991); *31* (8), 993-1008.

114. de Souza, L. E. S.; Ben-Amotz, D., Hard fluid model for molecular solvation free energies. *The Journal of Chemical Physics.* (1994); *101* (11), 9858-9863.

115. Shpiruk, T. A.; Khajehpour, M., The effect of urea on aqueous hydrophobic contact-pair interactions. *Physical Chemistry Chemical Physics* (2013); *15* (1), 213-222.

116. Ben-Naim, A., *Solvation thermodynamics*. Plenum Press: New York, (1987); p xi, 246 p.

117. Pratt, L. R.; Chandler, D., Theory of the hydrophobic effect *The Journal of Chemical Physics.* (1977); *67* (8), 3683-3704.

118. D. Ben-Amotz. Global thermodynamics of hydrophobic cavitation, dewetting, and hydration*. The Journal of Chemical Physics.* (2005); *123*, 184504.

119. Bondi, A. Van der Waals Volumes and Radii. *Journal of Physical Chemistry.* (1964); 68, 441-451.

120. Reiss, H., Scaled Particle Methods in the Statistical Thermodynamics of Fluids. In *Advances in Chemical Physics.* (1965); pp 1-84.

121. Desrosiers, N., Desnoyers, J. E., Enthalpies, heat capacities, and volumes of transfer of the tetrabutylammonium ion from water to aqueous mixed solvents from the point of view of the scaled-particle theory. *Canadian Journal of Chemistry.* (1976); *54* (23), 3800-3808.

122. Egorov, G. I., Makarov, D. M., Densities and Volumetric Properties of Aqueous Solutions of {Water (1) + N-Methylurea (2)} Mixtures at Temperatures of 274.15–333.15 K and at Pressures up to 100 MPa. *Journal of Chemical & Engineering Data.* (2017); *62* (12), 4383-4394.

123. Makarov, D. M., Egorov, G. I., Density and volumetric properties of the aqueous solutions of urea at temperatures from T = (278 to 333) K and pressures up to 100 MPa. *The Journal of Chemical Thermodynamics.* (2018); *120*, 164-173.

124. Belda Maximino, R. Surface tension and density of binary mixtures of monoalcohols, water and acetonitrile: equation of correlation of the surface tension. *Physics and Chemistry of Liquids*. (2009); 47:5, 475-486.

125. Krakowiak, J. Wawer, A. Panuszko. The hydration of the protein stabilizing agents: Trimethylamine-N-oxide, glycine and its N-methylderivatives – The volumetric and compressibility studies. *The Journal of Chemical Thermodynamics* (2013); *60*, 179-190.

126. C. Treiner, P. Tzias, M. Chemla, G. M. Poltoratskii. Solvation of tetrabutylammonium bromide in water + acetonitrile mixtures at 298.15 K from vapour pressure measurements of dilute solutions. *Journal of the Chemical Society, Faraday Transactions 1: Physical Chemistry in Condensed Phases.* (1976); *72*, 2007-2015.

127. D. M. Makarov, G. I. Egorov, A. M. Kolker. Density and Volumetric Properties of Aqueous Solutions of Trimethylamine N-Oxide in the Temperature Range from (278.15 to 323.15) K and at Pressures up to 100 MPa. *Journal of Chemical & Engineering Data.* (2015); *60*, 1291-1299.

128. Michael Heying, M., Corti, D.S. *Scaled Particle Theory Revisited: New Conditions and Improved Predictions of the Properties of the Hard Sphere Fluid. The Journal of Physical Chemistry B.* **(**2004); *108* (51), 19756-19768.

129. W. L. Jorgensen, J. Gao, C. Ravimohan, Monte Carlo simulations of alkanes in water: Hydration numbers and the hydrophobic effect. *The Journal of Physical Chemistry.* (1985); *89*, 3470-3473.

130. D. Ben-Amotz, F. O. Raineri, G. Stell. Solvation Thermodynamics: Theory and Applications. *The Journal of Physical Chemistry* B. (2005); 109, 6866-6878.

131. D. Ben-Amotz, K. G. Willis. Molecular Hard Sphere Volume Increments. *The Journal of Physical Chemistry.* (1993); *97*, 7736-7742.

132. G. Graziano. Salting out of methane by sodium chloride: A scaled particle theory study. *The Journal of Chemical Physics.* (2008); 129, 084506/084501-084506/084509.

133. O. A. Francisco, H. M. Glor, M. Khajehpour. Salt Effects on Hydrophobic Solvation: Is the Observed Salt Specificity the Result of Excluded Volume Effects or Water Mediated Ion-Hydrophobe Association? *ChemPhysChem* (2020); *21*, 484-493.

134. F. Avbelj, P. Luo, R. L. Baldwin. Hydration of the peptide backbone largely defines the thermodynamic propensity scale of residues at the C′ position of the C-capping box of α-helices. *Proceedings of the National Academy of Sciences* (2000); *97*, 10786-10791.

Chapter 4.

Conclusion & Future Directions

In this work we experimentally investigated how the addition of urea affects: a) the H-bonding properties of the solvent, b) the strength of an intra-molecular H-bond, and c) the solubility of the amide backbone. The effects of urea upon the H-bonding network of water were characterized by measuring how its addition perturbs the fluorescence spectrum of the probes 1-AN (a molecule that can donate and accept H-bonds) and 1-DMAN (a molecule that accepts only H-bonds) and compared with methanol and acetonitrile. Our spectral analysis of these two molecules not only confirms that urea has minimal effect on the H-bonding donation properties of the solvent [45,57,68], but interestingly also rules the possibility that urea significantly increases the H-bond acceptance of the solvent. The hypothesis that urea can directly break intra-molecular H-bonds [108], was investigated by studying its effects upon the pKa of salicylic acid (*o*-HBA). A comparison of the effects of urea with those of methanol clearly shows that the urea addition (unlike methanol) has no effect on the intra-molecular H-bond formed between the hydroxyl and carboxylate moieties (even at a urea concentration of 6 M, the magnitude of K_H remains unchanged compared with water). Finally, we quantify the effect of urea addition on the solubility of the amide groups by comparing its effect on the solubility of acetaminophen and 4-tertbutylphenol. Our data show that the effect of urea addition increases the solubility of the amide group and the energetics of this effect on solubility (unlike the addition of acetonitrile, which affects H-bonding) scales linearly with packing density. This behavior is a hallmark of van der Waals interactions between solvent and solute and experimentally demonstrates that the denaturation process of urea occurs through increasing van der Waals interactions between solvent and solute.

The work presented in this thesis has provided a molecular description for understanding the unfolding of proteins in urea-protein systems. Our research takes a reductionist approach, in which we simplify large, complex systems (e.g. protein unfolding in solution) into easily studied systems (solvation of probes representing protein moieties) where we are able to characterize the molecular interactions involved on a smaller scale, using biophysical models to explain our data as needed. Though we have made a significant contribution to the discussion, there is still room for improvement with more research, likely focusing on characterizing the unfolding mechanism of a protein as a whole biomolecule, rather than just looking at parts of the system. However, we have answered some interesting questions within our research scope pertaining to the denaturation mechanism of urea. Though urea as a protein denaturant was the main focus of my MSc. research, I have also worked on investigating the mechanisms of action of other important co-solvents on proteins in aqueous solvent systems, using the same model systems discussed in this study.

TMAO is a methylamine known to stabilize the native state of proteins and assist refolding of intrinsically-disordered proteins; counteracting the effects of urea on protein structure and biological activity [9,14]. Computational and theoretical work show that TMAO may inhibit protein backbone solvation possibly through stronger TMAO-solvent H-bonding interactions, while increasing the solvation of hydrophobic moieties in solution by reducing the magnitude of cavitation energy required for solvation [136-138]. However, this has not been firmly experimentally proven. Our solvatochromic (1-AN/1-DMAN) and amide solvation (ACT/TBP) studies show that TMAO reduces solvent H-bond donation to amide moieties, and at higher concentrations it increases solvent H-bond acceptance to amide moieties. This indicates that there is an optimal TMAO concentration at which it reinforces protein folding through reduction in solvent H-bond donation, without its effects on H-bond acceptance. A paper will be published on this work, in

which Dr. Khajehpour, Iman Asakareh and I are collaborating. The next experiments would aim to investigate whether TMAO enhances hydrophobic interactions by decreasing the magnitude of cavitation energy. Answering this question would provide clarity as to the mechanism of interaction of TMAO with its microenvironment.

Methanol as a co-solvent is also of interest in our research, as alcohols have been shown to induce the folding of disordered peptides into α-helical structures in aqueous solutions [19]. The findings of this work will be useful in characterizing the coil-helix folding transition of a model basic helix-loop-helix (bHLH) peptide, Rhau53 which is highly disordered in solution. Rhau53 was overexpressed in the lab with the help of Daniel Gussakovsky (McKenna Lab), and structural changes due to co-solvent addition were observed by far-UV circular dichroism (CD). Qualitatively, organic co-solvents (e.g. methanol) were shown to induce α-helicity in Rhau53 at high concentrations. This is largely due to the fact that methanol reinforces intramolecular H-bonding mainly through a reduction in solvent H-bond donation, as indicated from our solvatochromic (1-AN/1-DMAN) and pKa (*o*-HBA/*p*-HBA) studies. The data from these experiments will be quantitatively analyzed to determine the thermodynamic parameters of folding and other important terms. This work may also be published as a letter from Dr. Khajehpour, Iman Asakareh, Daniel Gussakovsky and I in the near future. Since the sequence and structure of bHLHs are highly conserved [139,140], the Rhau53 folding mechanism may serve as a model system to predict the folding conditions of other similar nucleic acid-binding bHLHs. All in all, our research provides a deeper understanding of how specific molecular interactions are important in the solvation of protein moieties, secondary structural elements (e.g., motifs, domains) and proteins in general. It may also provide fundamental insight on how and why various protein structures respond to changes in microenvironment.

References:

136. Ganguly, P. Protein stability in TMAO and mixed urea–TMAO solutions. *The Journal of Physical Chemistry. B*. (2020); 124 (29), 6181–6197.
137. Athawale, M. V. Osmolyte trimethylamine- N-oxide does not affect the strength of hydrophobic interactions: origin of osmolyte compatibility. *Biophysical Journal*. (2005); 89(2), 858–866.
138. Yang, Y. Microscopic significance of hydrophobic residues in the protein-stabilizing effect of trimethylamine-N-oxide (TMAO). *Physical Chemistry ChemicalPphysics : PCCP*. (2016); 18 (32), 22081–22088.
139. Jones, S. An overview of the basic helix-loop-helix proteins. *Genome Biology*. (2004); 5, 226.
140. Booy, E.P., Meier, M., Okun, N., Novakowski, S.K., Xiong, S., Stetefeld, J., McKenna, S.A. The RNA helicase RHAU (DHX36) unwinds a G4-quadruplex in human telomerase RNA and promotes the formation of the P1 helix template boundary. *Nucleic Acids Research*. (2012); 40(9), 4110-4124.